Received 22 September 2023; revised 13 November 2023; accepted 2 December 2023. Date of publication 6 December 2023; date of current version 29 December 2023.

Digital Object Identifier 10.1109/OJCOMS.2023.3340096

Decision Fusion in Centralized and Distributed Multiuser Millimeter-Wave Massive MIMO-OFDM Sensor Networks

PALLA SIVA KUMAR[1] (Student Member, IEEE), APOORVA CHAWLA[2] (Member, IEEE), SURAJ SRIVASTAVA[3] (Member, IEEE), ADITYA K. JAGANNATHAM[4] (Senior Member, IEEE), AND LAJOS HANZO[5] (Life Fellow, IEEE)

[1]Wireless R&D, Qualcomm India Private Ltd., Hyderabad 500081, India
[2]Department of Electronic Systems, Norwegian University of Science and Technology, 7491 Trondheim, Norway
[3]Department of Electrical Engineering, Indian Institute of Technology Jodhpur, Jodhpur 342030, India
[4]Department of Electrical Engineering, Indian Institute of Technology Kanpur, Kanpur 208016, India
[5]School of Electronics and Computer Science, University of Southampton, SO17 1BJ Southampton, U.K.

CORRESPONDING AUTHOR: L. HANZO (e-mail: lh@ecs.soton.ac.uk)

The work of Aditya K. Jagannatham was supported in part by the Qualcomm Innovation Fellowship; in part by the Qualcomm 6G UR Gift; and in part by the Arun Kumar Chair Professorship. The work of Lajos Hanzo was supported in part by the Engineering and Physical Sciences Research Council under Project EP/W016605/1, Project EP/X01228X/1, and Project EP/Y026721/1; and in part by the European Research Council's Advanced Fellow Grant QuantCom under Grant 789028.

This article has supplementary downloadable material available at https://doi.org/10.1109/OJCOMS.2023.3340096, provided by the authors.

ABSTRACT Low-complexity fusion rules relying on hybrid combining are proposed for decision fusion in frequency selective millimeter wave (mmWave) massive multiple-input multiple-output (MIMO) sensor networks (SNs). Both centralized (C-MIMO) and distributed (D-MIMO) antenna architectures are considered, where the error-prone local sensor decisions are transmitted over orthogonal subcarriers to a fusion center (FC) employing a large antenna array. Fusion rules are designed for the FC, followed by closed-form expressions of the false alarm and detection probabilities to comprehensively characterize the performance of distributed detection. Furthermore, efficient transmit signaling vectors are designed for optimizing the detection performance. Both the asymptotic performance analysis and the pertinent power reduction laws are presented for the large antenna regime considering both the C-MIMO and D-MIMO topologies, which potentially lead to a significant transmit power reduction. Low-complexity fusion rules and their analyses are also given for the realistic scenario of incorporating channel state information (CSI) uncertainty, where the sparse Bayesian learning (SBL) framework is utilized for the estimation of the sparse frequency selective mmWave massive MIMO channel. Finally, the performance of the proposed low-complexity detectors is characterized through extensive simulation results for different scenarios.

INDEX TERMS Decision fusion, millimeter wave, sparse Bayesian learning, OFDM, massive MIMO, hybrid combining, distributed detection.

I. INTRODUCTION

NEXT-GENERATION (NG) sensor networks (SNs) are envisaged to support ultra-dense sensor connectivity to enable real-time monitoring of a large area for mission-critical tasks in applications such as surveillance, disaster management, and agriculture, among others [1], [2], [3]. In these networks, battery-operated sensors are geographically distributed to monitor a specific event of interest. The sensor measurements are generally compressed into single-bit decisions, due to power and bandwidth constraints, and are subsequently transmitted to the fusion center (FC), where the final decision related to the presence/absence of a signal of interest is arrived at using a suitable fusion rule. This paradigm is referred to as distributed detection [4]. The rising interest in these applications both in current and NG networks, along with the drastic surge in the number

of miniature sensors has led to a spectrum-crunch in the sub-6 GHz bands. This motivates one to look for alternative frequency bands that can provide an abundance for spectrum necessary for NG SNs.

In this respect, millimeter wave (mmWave) communication serves as a potential technology for supporting high data rates and bandwidth-intensive applications by leveraging the underutilized band ranging from 30 to 300 GHz [5]. However, mmWave signals suffer from severe absorption and propagation losses, which renders the implementation of mmWave communication challenging [6]. To overcome this challenge, one can employ massive multiple-input multiple-output (MIMO) technology, wherein massive antenna arrays (AAs) are deployed at the base stations (BSs) within limited physical dimensions, thanks to the shorter wavelength of mmWave signals. This can play a pivotal role in compensating for the huge path losses at such higher frequencies, thus paving the way for the practical implementation of mmWave MIMO communication [7]. Furthermore, orthogonal frequency division multiplexing (OFDM), which provides robustness to inter-symbol interference (ISI) and multipath distortion, is well suited for mmWave massive MIMO SNs. Thus, mmWave massive MIMO-OFDM SNs constitute an effective solution for the reliable detection of events of critical importance in high-speed networks.

The conventional fully digital precoding/combining architectures employed in such systems, where the signal processing (SP) is exclusively executed in the baseband, necessitates a substantially larger number of radio frequency (RF) chains since an independent RF chain is required for each antenna. This fact, coupled with the high sampling rate of the ADCs due to the larger bandwidth of the signals, makes the system power-hungry and costly, precluding the deployment of fully digital signal processing (DSP) schemes in NG SNs. This issue can be circumvented by implementing the popular hybrid SP architecture [8], wherein SP tasks like analog/digital transmit precoding (TPC) and receiver combining are executed in the RF and baseband domains, respectively. Such architectures require only a modest number of RF chains in contrast to conventional fully DSP.

In a conventional mmWave massive MIMO SN, also known as centralized (C-MIMO) architecture, hundreds of antennas are co-located at the FC situated at the cell center. Despite having low deployment costs, this architecture experiences high spatial channel correlation and eventually leads to loss of orthogonality for the mmWave channels. To overcome this concern, distributed (D-MIMO) antenna configuration, wherein a very large AA is distributed over multiple geographically dispersed FCs that are linked together by a high-speed optical fiber backhaul, has gained considerable research interest [9]. Furthermore, the D-MIMO architecture potentially reduces the radio access distance between the sensors and the FCs, which facilitates significant power savings and improves the system performance over that of the C-MIMO architecture. The dense sensor deployment in NG networks naturally generates a tremendous amount of data that has to be processed to obtain reliable decisions regarding events of critical importance. Therefore, there is a crucial need to design efficient rules for decision fusion, which are investigated in this paper. A literature review is provided next.

A. LITERATURE REVIEW

Distributed detection for wireless sensor networks (WSNs) was first investigated by Li and Dai in their pioneering work in [10], wherein correlated observations were transmitted over a multiple access channel (MAC). The authors of [11] proposed modified amplify-and-forward (AF) and decode-and-forward (DF) based detection schemes for a MAC. A distributed detection algorithm was proposed and analyzed by Tepedelenlioglu and Dasarathan in [12] for a Gaussian MAC, wherein the sensor transmissions were constant modulus signals. Berger et al. [13] investigated the decentralized detection performance of MAC and parallel access channels (PAC) using noncoherent modulation. The optimality of the energy detector in the decision fusion was studied in [14] for a non-coherent Rayleigh fading MAC. In [15], Banavar et al. presented a novel AF-based distributed detection scheme for Ricean fading channels considering multiple antennas at the FC and characterized the performance of the system using an error exponent. This work was further extended in [16] to evaluate the optimal sensor transmit gains for different levels of channel state information (CSI) at the sensors. In [17], Ciuonzo et al. designed sub-optimal detection rules based on both the decode-and-fuse and decode-then-fuse principles for distributed MIMO SNs considering local decision transmission. The authors in [18] developed algorithms for distributed detection in WSNs considering both perfect and imperfect CSI both between the source and the sensors as well as between the sensors and the FC, followed by analyzing their performance in terms of the associated false alarm and detection probabilities. Novel DF relaying-based optimal and sub-optimal fusion rules were derived in [19] for cooperative WSNs. The authors of [20] successfully developed tests for multi-user (MU) cooperative MIMO spectrum sensing, incorporating realistic CSI uncertainty in the secondary user channels. The detection and estimation of a Gaussian signal in an AF WSN are investigated in [21] using both the energy and Neyman-Pearson (NP) detectors as well as the linear minimum mean-squared error estimator. In [22], Astaneh and Gazor studied the distributed detection performance of both the NP detector and of the generalized likelihood ratio test in an OFDM system. State-of-the-art detection rules were designed using the NP criterion in [23] for a massive MIMO-aided WSN, which also considers realistic imperfect CSI at the FC. In [24], a state of detection rules were developed for massive MIMO WSNs while considering both imperfect and perfect CSI availability, for both known/unknown parameter scenarios. A family of detection schemes were presented in [25] for mmWave massive C-MIMO WSNs for decision fusion, which were subsequently extended to the distributed antenna topology

TABLE 1. Contrasting our contributions to existing works.

	[14]	[17]	[18]	[19]	[21]	[33]	[23]	[24]	[30]	[9]	[25]	[28]	[32]	[38]	This work
Distributed detection analysis	✓	✓	✓	✓	✓	✓	✓	✓			✓	✓	✓		✓
mmWave communication									✓	✓	✓	✓		✓	✓
OFDM framework						✓							✓		✓
Amplify-and-forward			✓		✓			✓							
Local sensor decisions	✓	✓		✓		✓	✓				✓	✓	✓		✓
D-MIMO architecture									✓	✓				✓	✓
Optimal signaling	✓				✓				✓		✓	✓		✓	✓
Large-scale fading							✓	✓		✓	✓	✓		✓	✓
Asymptotic performance analysis					✓		✓	✓		✓				✓	✓
Power scaling laws					✓		✓	✓							✓
Linear detection							✓	✓			✓	✓	✓		✓
Practical FC selection algorithm										✓					✓
SBL-based channel estimation												✓			✓

in [26]. The sparse Bayesian learning (SBL) paradigm was proposed for sparse channel estimation in mmWave massive MIMO WSNs in [27], followed by the design of distributed detection schemes incorporating the associated CSI uncertainty in C- and D-MIMO architectures. Furthermore, the decision fusion in a mmWave massive MIMO WSN is investigated in [28], harnessing the SBL framework for realistic imperfect channel estimation. However, the analysis is restricted only to the centralized antenna architecture, where the sensors transmit their decisions to the FC over a flat fading channel. In [29], Gimenez et al. characterized the performance of a distributed hybrid precoding algorithm designed for a mmWave D-MIMO system in an indoor setting. Hybrid transmit/receive beamforming schemes were presented in [30] for heterogeneous systems to mitigate the inter- and intra-tier interferences in mmWave massive MIMO scenarios. In [9], the authors investigated the asymptotic spectral efficiencies of the MU mmWave massive MIMO downlink (DL) employing a hybrid precoding algorithm for C- and D-MIMO topologies. The authors of [31] proposed a cooperative MIMO-OFDM algorithm for enhancing energy efficiency and for interference mitigation in multi-hop 3D wireless camera SNs. Al-Jarrah et al. [32] studied parallel distributed detection in a WSN conceived for the local sensor decisions' transmission to the FC using a cooperative transmission strategy, where the FC receives each local decision as an OFDM block. The authors of [33] designed fusion rules for distributed detection by exploiting the probability density function (PDF) of the received signal, for an OFDM system. However, to the best of our knowledge, none of the existing treatises have proposed hybrid combining-based fusion rules for a WSN, where the sensors transmit their local decisions over frequency selective channels while leveraging the benefits of mmWave massive MIMO technologies. Hence, this paper explores the problem of distributed detection in an OFDM-based mmWave massive MIMO WSN, wherein the sensors transmit their decisions over orthogonal subcarriers. Table 1 contrasts the key features of the paper vis-à-vis those of the closely related works reviewed above. The detailed contributions of this work are further detailed below.

B. KEY CONTRIBUTIONS

- This study investigates an OFDM system wherein the sensors transmit their local decisions over single/multiple orthogonal subcarriers to the FC over a frequency selective mmWave massive MIMO channel. This scenario is in contrast to [15], [16], [24], [27] and [34], where analog observations are transmitted. Fusion rules are conceived for processing the wideband signal received at the FC, to determine a global decision.
- Low-complexity detection rules based on hybrid receiver combining (RC) are designed for C- and D-MIMO antenna topologies for antipodal signaling and low signal-to-noise ratios (SNR). Closed-form expressions of the false alarm (P_{FA}) and detection (P_D) probabilities are for characterizing the system performance.
- Furthermore, a beneficial signaling vector design is conceived for the D- and C-MIMO topologies in order to improve the detection performance.
- The asymptotic performance analysis and the associated power reduction laws are determined for a large number of antennas. The analysis clearly demonstrates the substantial sensor transmit power reduction attained without affecting the detection performance, thereby resulting in improved battery life.
- The extension of the above framework to a realistic scenario incorporating CSI uncertainty is also investigated. The SBL approach [35], [36] is utilized for exploiting the sparsity of the mmWave channel to obtain improved estimates of the frequency selective mmWave massive MIMO-OFDM CSI. It is a promising sparse signal recovery method, which has also shown superior performance compared to various state-of-the-art schemes in our recent work related to delay-Doppler domain sparse CSI estimation [37]. Furthermore, suitable hybrid combining-based fusion rules are designed for both antenna topologies under realistic imperfect CSI.

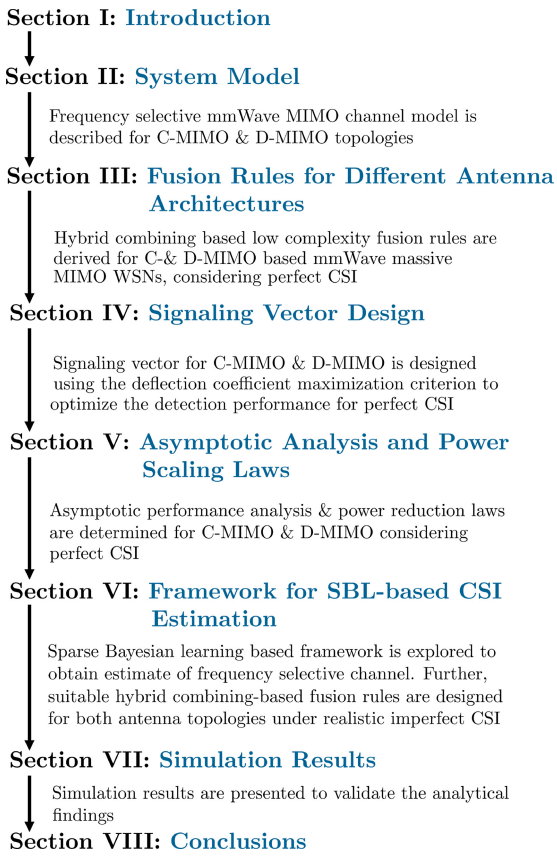

FIGURE 1. Flow of the paper.

- Simulation results are provided for validating the theoretical findings for characterizing the performance of the proposed novel detectors.

C. ORGANIZATION

The organization of the paper is as follows. Section II discusses the system model of mmWave C- and D- massive MIMO-OFDM SNs. The fusion rules are determined in Section III and our signaling vector design procedure is described in Section IV. The asymptotic performance and the associated power reduction laws are analyzed in Section V. Furthermore, our novel SBL-based channel estimation scheme and the corresponding fusion rules are given in Section VI. Finally, our simulation results and conclusions are provided in Sections VII and VIII, respectively. Furthermore, we have provided a diagram, depicted in Fig. 1, to concisely outline the contributions in each section.

D. NOTATIONS

Boldface uppercase (resp. lowercase) letters denote matrices and vectors, where $[\mathbf{X}]_{i,j}$ is the (i,j)th entry of $\mathbf{X}$ and x_i is the ith entry of $\mathbf{x}$, $\mathbf{0}_K$ and $\mathbf{I}_K$ are the $K \times 1$ zero vector and $K \times K$ identity matrix, respectively, $\Re(.)$, $\mathbb{E}\{.\}$, $\exp(.)$, $o(.)$, $\mathcal{O}(.)$, $(.)^H$, $(.)^T$, $\lfloor\rfloor$, $\otimes$, $(.)^*$, $\|.\|$, represent the real part, expectation operator, exponential function, little o, big O, conjugate transpose, transpose, floor, Kronecker product, conjugate, and Euclidean norm, respectively, $p(.)$, $p(.|.)$, $\Pr(.)$ and $\Pr(.|.)$ denote the PDF, conditional PDF, probability and conditional probability, respectively.

II. SYSTEM MODEL

Consider K single-antenna sensors which are randomly distributed in a mmWave massive MIMO SN to sense the presence ($\mathcal{H}_1$) (resp. absence ($\mathcal{H}_0$)) of a signal of interest. The sensors subsequently send their local decisions to either a single FC or multiple FCs, depending on the antenna configuration, over a frequency selective fading channel. Let N_s successive subcarriers be allocated to each sensor and the same signal be transmitted over all the N_s subcarriers, so that beneficial frequency diversity is attained. Hence, the signal corresponding to the kth sensor, $0 \leq k \leq K-1$, becomes:

$$\tilde{x}_k(n) = \sum_{i=0}^{N_s-1} x_k e^{j\frac{2\pi}{N}(kN_s+i)n}, \forall 0 \leq n \leq N-1, \tag{1}$$

where $N = N_s K$ is the total number of subcarriers. For antipodal signaling, the local decision x_k corresponding to the kth sensor belongs to the set $x_k \in \{u_k, -u_k\}$, so that its local false alarm and detection probabilities can be expressed as $P_{F,k} = \Pr(x_k = u_k|\mathcal{H}_0)$ and $P_{D,k} = \Pr(x_k = u_k|\mathcal{H}_1)$. Subsequently, the signals of the K sensors are processed at the FC to obtain a final decision. The frequency selective mmWave MIMO channel models for different antenna topologies are discussed next.

A. FREQUENCY SELECTIVE MMWAVE MIMO CHANNEL MODEL

In the C-MIMO configuration, the sensors transmit their local decisions to a single FC, located at the center of the cell. The FC is equipped with a massive antenna array (AA) containing M antennnas. The centralized antenna topology is depicted in Fig. 2a. Considering the D-delay channel model of [39] for the C-MIMO topology, the d-th delay tap $\mathbf{g}_{k,d} \in \mathbb{C}^{M\times 1}$ associated with the kth sensor and the FC is $\mathbf{g}_{k,d} = \sqrt{\beta_k}\mathbf{h}_{k,d}$, $\forall\ k$, where β_k characterizes the pathloss and log-normal shadowing [40], while $\mathbf{h}_{k,d}$ is the small-scale fading vector [41] modeled as

$$\mathbf{h}_{k,d} = \sqrt{\frac{M}{L_k}} \sum_{i=0}^{L_k-1} \tilde{\alpha}_k^i \mathbf{a}_r(\theta_k^i) p_k(dT_s - \tau_{k,i}), \tag{2}$$

where $\tau_{k,i}$ and $\tilde{\alpha}_k^i$ are the delay and complex channel gains of the kth sensor and the ith spatial multipath component, respectively. The parameters T_s, L_k, and $p_k(\tau)$ denote the sampling period, the number of multipath components, and the band-limited pulse shaping filter response at delay τ, respectively. The receive array response vector $\mathbf{a}_r(\theta_k^i) \in \mathbb{C}^{M\times 1}$ is defined as $\mathbf{a}_r(\theta_k^i) = \frac{1}{\sqrt{M}}[1, e^{j\frac{2\pi}{\lambda}d\sin(\theta_k^i)}, \ldots, e^{j\frac{2\pi}{\lambda}d(M-1)\sin(\theta_k^i)}]^T$, where θ_k^i is the angle of arrival (AoA) of the ith multipath and the kth sensor, while λ, and d denote the wavelength and receive antenna spacing,

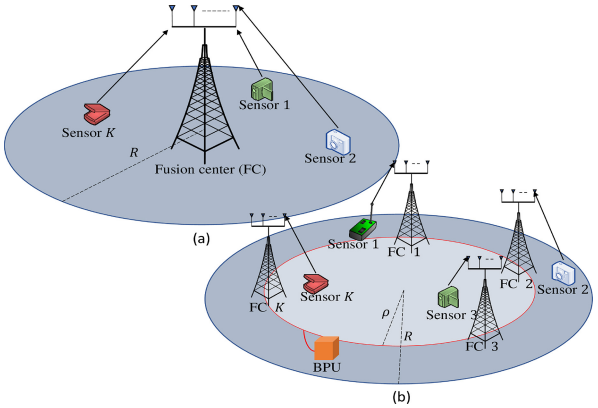

FIGURE 2. Antenna topologies of mmWave massive MIMO-OFDM SN (a) Centralized (b) Distributed.

respectively. In the frequency domain, the lth subcarrier channel vector $\mathbf{g}_l \in \mathbb{C}^{M\times 1}$ is derived as

$$\mathbf{g}_l = \sum_{d=0}^{D-1} \mathbf{g}_{k,d} e^{-j\frac{2\pi}{N}kd}, \quad \forall \;\; 0 \le l \le N-1, \tag{3}$$

where the variable k satisfies $k = \lfloor \frac{l}{N_s} \rfloor$, with a total of N_s consecutive subcarriers allocated to the kth sensor and the channel assumed to be constant across the N_s subcarriers. Using (3), the channel vector $\mathbf{g}_l$ can be remodeled as $\mathbf{g}_l = \sqrt{\frac{M\beta_k}{L_k}}\mathbf{A}_{r,k}\boldsymbol{\alpha}_l$, where $\boldsymbol{\alpha}_l \in \mathbb{C}^{L_k\times 1}$ and $\mathbf{A}_{r,k} \in \mathbb{C}^{M\times L_k}$ denote the equivalent complex channel gain vector associated with the kth sensor and the lth subcarrier and the receive array response matrix of the kth sensor, respectively.

In the D-MIMO architecture, J FCs are uniformly distributed on a circle of radius ρ with R being the cell radius. All the J FCs are interconnected via the high-capacity and low-latency backhaul infrastructure constituted by optical fiber cables. Each FC is equipped with an independent N_d-element AA, hence the total number of antennas N_{tot} across all FCs is $N_{tot} = N_d J$. Additionally, each FC utilizes a single RF chain connected to its N_d-element AA. The RF combiner outputs from all the FCs are then directed to the baseband processing unit (BPU) for further signal processing, as illustrated in Fig. 2b. The circular layout is preferred because of its compatibility with the existing infrastructure and low optical backhaul installation requirements [9]. To ensure a fair comparison with C-MIMO, it is assumed that $N_{tot} = M$ and $J = K$, similar to the model in [9]. For D-MIMO, the channel vector related to the l_kth subcarrier and the jth FC is formulated as

$$\mathbf{g}_{l_k,j} = \sqrt{\frac{N_d\beta_{k,j}}{L_{k,j}}}\mathbf{A}_{r,k,j}\boldsymbol{\alpha}_{l_k,j}, \tag{4}$$

where $l_k \in \mathbb{A}_k = \{kN_s, kN_s+1, \ldots, (k+1)N_s-1\}$. The quantities $\mathbf{A}_{r,k,j} \in \mathbb{C}^{N_d\times L_{k,j}}$, $\beta_{k,j}$ and $L_{k,j}$ represent the receive array response matrix, large-scale fading coefficient and the number of multipath components, respectively, for the kth sensor and the jth FC. Furthermore, $\boldsymbol{\alpha}_{l_k,j} \in \mathbb{C}^{L_{k,j}\times 1}$, $\forall l_k \in \mathbb{A}_k$, is the equivalent complex channel gain vector of the jth FC, l_kth subcarrier and the kth sensor. The decision rules for the C- and D-MIMO topologies, considering perfect CSI, are described in the subsequent section.

III. FUSION RULES FOR DIFFERENT ANTENNA ARCHITECTURES

In this section, fusion rules are developed for both antenna configurations, considering hybrid combining and perfect CSI at the FC. Next, the decision rule for the centralized architecture is discussed.

A. DECISION RULE FOR A C-MIMO BASED WSN

After the N-point fast Fourier transform (FFT) of OFDM, the signal $\mathbf{y}(l) \in \mathbb{C}^{M\times 1}$ received at the FC corresponding to the lth subcarrier becomes

$$\mathbf{y}(l) = \sqrt{p_u}\mathbf{g}_l x_k + \mathbf{w}(l), \tag{5}$$

where the additive white Gaussian noise (AWGN) $\mathbf{w}(l) \in \mathbb{C}^{M\times 1}$ is distributed as $\mathbf{w}(l) \sim \mathcal{CN}(\mathbf{0}, \sigma_w^2\mathbf{I}_M)$. After stacking N_s outputs of the kth sensor, one obtains the equivalent received signal vector $\mathbf{y}_k = [\mathbf{y}^T(kN_s), \ldots, \mathbf{y}^T((k+1)N_s-1)]^T \in \mathbb{C}^{MN_s\times 1}$ as

$$\mathbf{y}_k = \sqrt{p_u}\mathbf{g}_k x_k + \mathbf{w}_k, \tag{6}$$

where $\mathbf{g}_k = [\mathbf{g}^T(kN_s), \ldots, \mathbf{g}^T((k+1)N_s-1)]^T \in \mathbb{C}^{MN_s\times 1}$ is the equivalent channel vector and the equivalent noise vector $\mathbf{w}_k = [\mathbf{w}^T(kN_s), \ldots, \mathbf{w}^T((k+1)N_s-1)]^T \in \mathbb{C}^{MN_s\times 1}$ is distributed as $\mathbf{w}_k \sim \mathcal{CN}(\mathbf{0}, \mathbf{C}_\mathbf{w})$, where $\mathbf{C}_\mathbf{w} = \sigma_w^2\mathbf{I}_{MN_s}$. Furthermore, the above signal $\mathbf{y}_k$ is distributed as $\mathbf{y}_k \sim \mathcal{CN}(\boldsymbol{\mu}_{\mathbf{y}_k}, \mathbf{C}_\mathbf{w})$, where the mean $\boldsymbol{\mu}_{\mathbf{y}_k}$ is defined as $\boldsymbol{\mu}_{\mathbf{y}_k} = \sqrt{p_u}\mathbf{g}_k x_k$. Upon concatenating the output vectors of all K sensors, one obtains

$$\mathbf{Y} = \sqrt{p_u}\mathbf{G}\mathbf{X} + \mathbf{W}, \tag{7}$$

where $\mathbf{Y} = [\mathbf{y}_0, \ldots, \mathbf{y}_{K-1}] \in \mathbb{C}^{MN_s\times K}$, $\mathbf{G} = [\mathbf{g}_0, \ldots, \mathbf{g}_{K-1}] \in \mathbb{C}^{MN_s\times K}$, $\mathbf{X} = \text{diag}(x_0, \ldots, x_{K-1}) \in \mathbb{C}^{K\times K}$ and $\mathbf{W} = [\mathbf{w}_0, \ldots, \mathbf{w}_{K-1}] \in \mathbb{C}^{MN_s\times K}$ denote the equivalent received signal, channel, transmitted signal and noise matrices, respectively.

Upon using the NP criterion, the log-likelihood ratio (LLR) test [42] for the scenario considering the C-MIMO configuration and perfect CSI can be formulated as

$$\begin{aligned} T_{\text{CP}}(\mathbf{Y}) &= \ln\left[\frac{p(\mathbf{Y}|\mathcal{H}_1)}{p(\mathbf{Y}|\mathcal{H}_0)}\right] \\ &= \sum_{k=0}^{K-1} \ln\left[\frac{\sum_{x_k} p(\mathbf{y}_k|x_k)\Pr(x_k|\mathcal{H}_1)}{\sum_{x_k} p(\mathbf{y}_k|x_k)\Pr(x_k|\mathcal{H}_0)}\right] \underset{\mathcal{H}_0}{\overset{\mathcal{H}_1}{\gtrless}} \gamma. \end{aligned} \tag{8}$$

Note that the expression in (8) is obtained by exploiting the independence of $\mathbf{y}_k$ across different sensors. For antipodal signaling, the LLR test reduces to

$$T_{\text{CP}}(\mathbf{Y}) = \sum_{k=0}^{K-1} \ln\left[\frac{\sum_{x_k} \exp\left(-\frac{\|\mathbf{y}_k - \boldsymbol{\mu}_{\mathbf{y}_k}\|^2}{\sigma_w^2}\right)\Pr(x_k|\mathcal{H}_1)}{\sum_{x_k} \exp\left(-\frac{\|\mathbf{y}_k - \boldsymbol{\mu}_{\mathbf{y}_k}\|^2}{\sigma_w^2}\right)\Pr(x_k|\mathcal{H}_0)}\right]. \tag{9}$$

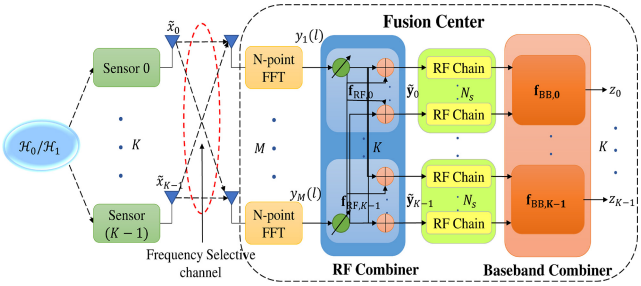

FIGURE 3. Hybrid combining based system model for decision fusion in the C-MIMO configuration.

Notice that the simplification of the above expression requires the addition of a large number of exponential terms. Hence, the above test statistic is computationally complex and unsuitable for light-weight practical implementation. To mitigate this concern, a hybrid combining-based two-step procedure is utilized for approximating the test in (8) [25], as illustrated in Fig. 3. In the first step, the received signal is processed by an analog RC $\mathbf{f}_{\mathrm{RF},l} \in \mathbb{C}^{M\times 1}$, followed by the digital RC $\mathbf{f}_{\mathrm{BB},k} \in \mathbb{C}^{N_s\times 1}$ in the next step. After that, the hybrid RC outputs are processed to form a global decision.

The RF combiner for the kth sensor is chosen as $\mathbf{f}_{\mathrm{RF},l} = \mathbf{a}_r(\theta_k^{i_k})$, which is the receive array response vector of the path having the maximum gain and i_k is the corresponding index. After RF combining, the processed signal $\tilde{y}(l)$ is given by $\tilde{y}(l) = \sqrt{p_u}\mathbf{f}_{\mathrm{RF},l}^H\mathbf{g}_l x_k + \tilde{w}(l)$, where the equivalent noise is $\tilde{w}(l) = \mathbf{f}_{\mathrm{RF},l}^H\mathbf{w}(l) \sim \mathcal{CN}(0,\sigma_w^2)$. Upon exploiting the asymptotic orthogonality of the mmWave massive MIMO channels [43] formulated as:

$$\mathbf{a}_r^H\left(\theta_m^{i_s}\right)\mathbf{a}_r\left(\theta_n^{i_t}\right) = \begin{cases} 1, & s = t \text{ and } m = n \\ 0, & s \neq t \text{ or } m \neq n \end{cases}, \tag{10}$$

the quantity $\mathbf{f}_{\mathrm{RF},l}^H\mathbf{g}_l$ reduces to $\mathbf{f}_{\mathrm{RF},l}^H\mathbf{g}_l = \sqrt{\frac{M\beta_k}{L_k}}\alpha_l^{i_k}$. Hence, the RF combiner output $\tilde{\mathbf{y}}_k = [\tilde{y}(kN_s),\ldots,\tilde{y}((k+1)N_s-1)]^T \in \mathbb{C}^{N_s\times 1}$, of the kth sensor corresponding to N_s subcarriers, is

$$\tilde{\mathbf{y}}_k = \sqrt{p_u}\sqrt{\frac{M\beta_k}{L_k}}\boldsymbol{\alpha}_k x_k + \tilde{\mathbf{w}}_k, \tag{11}$$

where $\boldsymbol{\alpha}_k = [\alpha_{kN_s}^{i_k},\ldots,\alpha_{(k+1)N_s-1}^{i_k}]^T \in \mathbb{C}^{N_s\times 1}$ and $\tilde{\mathbf{w}}_k = [\tilde{w}(kN_s),\ldots,\tilde{w}((k+1)N_s-1)]^T \in \mathbb{C}^{N_s\times 1}$ are the equivalent channel gain and noise vectors, respectively. Furthermore, the baseband RC is selected as $\mathbf{f}_{\mathrm{BB},k} = \sqrt{\frac{M\beta_k}{L_k}}\boldsymbol{\alpha}_k$, which aims for maximizing the signal's SNR. Hence, the baseband RC output z_k is obtained as

$$z_k = \sqrt{p_u}Md_k x_k + w_k, \tag{12}$$

where $d_k = \frac{\beta_k}{L_k}\|\boldsymbol{\alpha}_k\|^2$ and $w_k = \sqrt{\frac{M\beta_k}{L_k}}\boldsymbol{\alpha}_k^H\tilde{\mathbf{w}}_k$ is distributed as $w_k \sim \mathcal{CN}(0,\sigma_k^2)$ with $\sigma_k^2 = Md_k\sigma_w^2$. Moreover, the hybrid combiner output z_k is distributed as $z_k \sim \mathcal{CN}(\sqrt{p_u}Md_kx_k,\sigma_k^2)$. For the centralized mmWave massive MIMO-OFDM WSN, the LLR test based on the hybrid combiner output $\mathbf{z}$ can be simplified to

$$T_{\mathrm{CP}}(\mathbf{z}) = \sum_{k=0}^{K-1}\ln\left[\frac{P_{D,k}+(1-P_{D,k})\exp\left(-\frac{4\sqrt{p_u}\Re(z_k^*u_k)}{\sigma_w^2}\right)}{P_{F,k}+(1-P_{F,k})\exp\left(-\frac{4\sqrt{p_u}\Re(z_k^*u_k)}{\sigma_w^2}\right)}\right]. \tag{13}$$

Under the low SNR assumption, the test in (13) reduces to

$$T_{\mathrm{CP}}(\mathbf{z}) = \sum_{k=0}^{K-1}a_k\Re(z_k^*u_k) \underset{\mathcal{H}_0}{\overset{\mathcal{H}_1}{\gtrless}} \gamma', \tag{14}$$

where $a_k \triangleq P_{D,k} - P_{F,k}$. The above expression follows from the approximations $e^{-s} \approx 1-s$ and $\ln(1+s) \approx s$. Observe that the detector in (14) has low complexity in contrast to the fusion rule in (9), which requires the addition of a large number of exponential terms. Moreover, the proposed detector is suitable for practical scenarios, since WSNs are typically resource-constrained. Furthermore, $T_{\mathrm{CP}}(\mathbf{z})$ in (14) is a complex Gaussian random variable since it is a weighted sum of K complex Gaussian random variables. For a scenario wherein the sensors have the same local false alarm and detection probabilities, i.e., $P_{F,k} = P_f$ and $P_{D,k} = P_d, \forall\ k$, the test in (14) simplifies to $T_{\mathrm{CP,I}}(\mathbf{z}) = \sum_{k=0}^{K-1}\Re(z_k^*u_k) \underset{\mathcal{H}_0}{\overset{\mathcal{H}_1}{\gtrless}} \gamma'$. The performance of the test in (14) is presented next.

Theorem 1: Considering the C-MIMO architecture of our mmWave massive MIMO-OFDM WSN, the detection (P_D) and false alarm (P_{FA}) probabilities of the test $T_{\mathrm{CP}}(\mathbf{z})$ in (14) are

$$P_D = Q\left(\frac{\gamma' - \mu_{T_{\mathrm{CP}}|\mathcal{H}_1}}{\sigma_{T_{\mathrm{CP}}|\mathcal{H}_1}}\right), P_{FA} = Q\left(\frac{\gamma' - \mu_{T_{\mathrm{CP}}|\mathcal{H}_0}}{\sigma_{T_{\mathrm{CP}}|\mathcal{H}_0}}\right),$$

where the means $\mu_{T_{\mathrm{CP}}|\mathcal{H}_0}$, $\mu_{T_{\mathrm{CP}}|\mathcal{H}_1}$ and the variances $\sigma^2_{T_{\mathrm{CP}}|\mathcal{H}_0}$, $\sigma^2_{T_{\mathrm{CP}}|\mathcal{H}_1}$ under the $\mathcal{H}_0$ and $\mathcal{H}_1$ hypotheses, respectively, are

$$\mu_{T_{\mathrm{CP}}|\mathcal{H}_0} = \sum_{k=0}^{K-1}\sqrt{p_u}Ma_kd_kc_k|u_k|^2, \tag{15}$$

$$\mu_{T_{\mathrm{CP}}|\mathcal{H}_1} = \sum_{k=0}^{K-1}\sqrt{p_u}Ma_kd_kb_k|u_k|^2, \tag{16}$$

$$\sigma^2_{T_{\mathrm{CP}}|\mathcal{H}_0} = \sum_{k=0}^{K-1}Ma_k^2d_k|u_k|^2\left(p_uMd_k|u_k|^2(1-c_k^2)+\frac{\sigma_w^2}{2}\right), \tag{17}$$

$$\sigma^2_{T_{\mathrm{CP}}|\mathcal{H}_1} = \sum_{k=0}^{K-1}Ma_k^2d_k|u_k|^2\left(p_uMd_k|u_k|^2(1-b_k^2)+\frac{\sigma_w^2}{2}\right), \tag{18}$$

where $c_k = 2P_{F,k}-1$ and $b_k = 2P_{D,k}-1$.

Proof: See Appendix A. ■

The fusion rule for the distributed antenna architecture is discussed next.

B. DECISION RULE FOR A D-MIMO BASED WSN

In the D-MIMO architecture, the task of assigning sensors to the operating FCs is crucial, hence diverse FC selection

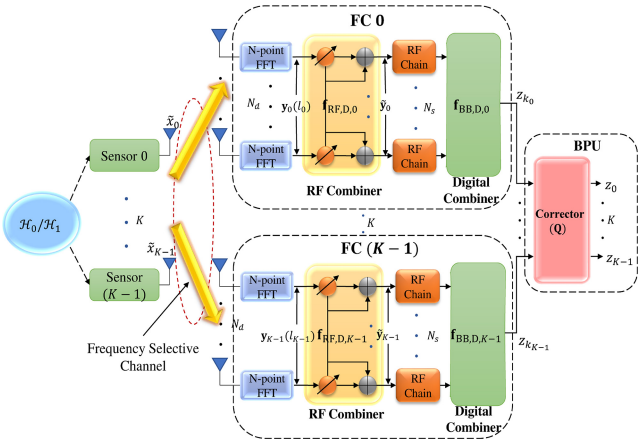

FIGURE 4. Hybrid combining based system model for decision fusion in the D-MIMO topology.

algorithms have been developed in [9]. The distance (D)-based algorithm, where an sensor is allocated to its nearest FC according to the minimum distance criterion, is widely used in the literature [9]. Hence, we also employ the D-based algorithm to design detectors for the distributed antenna architecture. To implement the D-based algorithm, a distance matrix $\mathbf{D} \in \mathbb{R}^{K\times J}$ is determined so that its (k,j)th entry $d_{k,j} = [\mathbf{D}]_{k,j}$ denotes the distance of the kth sensor from the jth FC. Let $\mathbf{S} \in \mathbb{R}^{K\times J}$ be the binary correction matrix, where $[\mathbf{S}]_{k,j} = 1$, when the jth FC is assigned to the kth sensor and $[\mathbf{S}]_{k,j} = 0$, otherwise. Furthermore, $\mathbf{S}^H\mathbf{S} = \mathbf{I}_K$ since only a single sensor is allocated to each FC and $J = K$.

For the D-MIMO topology, the signal received at the jth FC $\mathbf{y}_j(l_j) \in \mathbb{C}^{N_d\times 1}$ corresponding to the l_jth subcarrier is $\mathbf{y}_j(l_j) = \sqrt{p_u}\mathbf{g}_{l_j,j}x_{k_j} + \mathbf{w}_j(l_j)$, where $l_j \in \mathbb{A}_{k_j}$, $\mathbb{A}_{k_j} = \{k_jN_s, k_jN_s{+}1, \ldots, (k_j{+}1)N_s{-}1\}$, the AWGN $\mathbf{w}_j(l_j) \in \mathbb{C}^{N_d\times 1}$ is distributed as $\mathbf{w}_j(l_j) \sim \mathcal{CN}(\mathbf{0}, \sigma_w^2\mathbf{I}_{N_d})$ and the channel vector $\mathbf{g}_{l_j,j}$ is defined as $\mathbf{g}_{l_j,j} = \sqrt{\frac{N_d\beta_{k_j,j}}{L_{k_j,j}}}\mathbf{A}_{r,k_j,j}\boldsymbol{\alpha}_{l_j,j}, \forall l_j \in \mathbb{A}_{k_j}$. Similarly, a two-step architecture is utilized for the D-MIMO based WSN to reduce the computational complexity of the LRT, as demonstrated in Fig. 4. For the jth FC and the k_jth sensor, the RF combiner $\mathbf{f}_{\mathrm{RF},\mathrm{D},j} \in \mathbb{C}^{N_d\times 1}$ is chosen as $\mathbf{f}_{\mathrm{RF},\mathrm{D},j} = \mathbf{a}_r(\theta_{k_j,j}^{i_{k_j}}), \forall l_j$, which represents the receive array response vector with maximum path gain. Hence, the output of the RF combiner can be expressed as

$$\tilde{y}_j(l_j) = \sqrt{p_u}\mathbf{f}_{\mathrm{RF},\mathrm{D},j}^H\mathbf{g}_{l_j,j}x_{k_j} + \tilde{w}_j(l_j), \tag{19}$$

where the noise $\tilde{w}_j(l_j) = \mathbf{f}_{\mathrm{RF},\mathrm{D},j}^H\mathbf{w}_j(l_j)$ is distributed as $\tilde{w}_j(l_j) \sim \mathcal{CN}(0, \sigma_w^2)$. Furthermore, observe that the quantity $\mathbf{f}_{\mathrm{RF},\mathrm{D},j}^H\mathbf{g}_{l_j,j}$ reduces to $\sqrt{\frac{N_d\beta_{k_j,j}}{L_{k_j,j}}}\alpha_{l_j,j}^{i_{k_j}}$. After stacking the RF combiner outputs corresponding to the k_jth sensor, one obtains

$$\tilde{\mathbf{y}}_j = \sqrt{p_u}\sqrt{\frac{N_d\beta_{k_j,j}}{L_{k_j,j}}}\boldsymbol{\alpha}_j x_{k_j} + \tilde{\mathbf{w}}_j, \tag{20}$$

where $\tilde{\mathbf{y}}_j \in \mathbb{C}^{N_s\times 1}$ and $\boldsymbol{\alpha}_j \in \mathbb{C}^{N_s\times 1}$ denote the equivalent RF combiner output vector and the channel gain vector associated with the jth FC, respectively. The equivalent noise vector $\tilde{\mathbf{w}}_j \in \mathbb{C}^{N_s\times 1}$ follows the Gaussian normal distribution, which is given as $\tilde{\mathbf{w}}_j \sim \mathcal{CN}(\mathbf{0}, \sigma_w^2\mathbf{I}_{N_s})$. Furthermore, to maximize the SNR at the jth FC, the baseband combiner is chosen as $\mathbf{f}_{\mathrm{BB},\mathrm{D},j} = \sqrt{\frac{N_d\beta_{k_j,j}}{L_{k_j,j}}}\boldsymbol{\alpha}_j$. Therefore, the hybrid combiner output z_{k_j} at the jth FC is

$$z_{k_j} = \sqrt{p_u}N_d d_{k_j,j}x_{k_j} + w_{k_j}, \tag{21}$$

where the quantity $d_{k_j,j}$ is defined as $d_{k_j,j} = \frac{\beta_{k_j,j}}{L_{k_j,j}}\|\boldsymbol{\alpha}_j\|^2$ and the equivalent noise w_{k_j} is distributed as $w_{k_j} \sim \mathcal{CN}(0, \sigma_{k_j}^2)$ with $\sigma_{k_j}^2 = N_d d_{k_j,j}\sigma_w^2$. The hybrid combiner outputs gleaned from K FCs are processed using the correction matrix $\mathbf{S}$ at the baseband processing unit (BPU) to derive the soft decisions of all sensors. The kth sensor soft decision is

$$z_k = \sqrt{p_u}N_d d_{k,j_k}x_k + w_k, \tag{22}$$

which is distributed as $z_k \sim \mathcal{CN}(\sqrt{p_u}N_d d_{k,j_k}x_k, \sigma_k^2)$, where $\sigma_k^2 = N_d d_{k,j_k}\sigma_w^2$. Considering the D-MIMO topology, the LLR test of mmWave massive MIMO-OFDM based WSNs can be expressed as

$$T_{\mathrm{DP}}(\mathbf{z}) = \sum_{k=0}^{K-1}\ln\left[\frac{P_{D,k}+(1-P_{D,k})\exp\left(-\frac{4\sqrt{p_u}\Re(z_k^*u_k)}{\sigma_w^2}\right)}{P_{F,k}+(1-P_{F,k})\exp\left(-\frac{4\sqrt{p_u}\Re(z_k^*u_k)}{\sigma_w^2}\right)}\right]. \tag{23}$$

Furthermore, for the low SNR regime, the above test reduces to

$$T_{\mathrm{DP}}(\mathbf{z}) = \sum_{k=0}^{K-1} a_k\Re(z_k^*u_k) \underset{\mathcal{H}_0}{\overset{\mathcal{H}_1}{\gtrless}} \tilde{\gamma}, \tag{24}$$

where $\tilde{\gamma}$ is the threshold. Since, the test in (24) is a weighted linear combination of Gaussian random variables, the test statistic $T_{\mathrm{DP}}(\mathbf{z})$ is complex Gaussian distributed. The performance of the test in (24) is presented next.

Theorem 2: For the test $T_{\mathrm{DP}}(\mathbf{z})$ in (24), the detection (P_D) and false alarm (P_{FA}) probabilities used for decision fusion at the mmWave distributed massive MIMO-OFDM based WSNs, are

$$P_D = Q\left(\frac{\tilde{\gamma}-\mu_{T_{\mathrm{DP}}|\mathcal{H}_1}}{\sigma_{T_{\mathrm{DP}}|\mathcal{H}_1}}\right), P_{FA} = Q\left(\frac{\tilde{\gamma}-\mu_{T_{\mathrm{DP}}|\mathcal{H}_0}}{\sigma_{T_{\mathrm{DP}}|\mathcal{H}_0}}\right),$$

where the means $\mu_{T_{\mathrm{DP}}|\mathcal{H}_0}$, $\mu_{T_{\mathrm{DP}}|\mathcal{H}_1}$ and the variances $\sigma_{T_{\mathrm{DP}}|\mathcal{H}_0}^2$, $\sigma_{T_{\mathrm{DP}}|\mathcal{H}_1}^2$ of $T_{\mathrm{DP}}(\mathbf{z})$ under hypotheses $\mathcal{H}_0$ and $\mathcal{H}_1$, respectively, are given as

$$\mu_{T_{\mathrm{DP}}|\mathcal{H}_0} = \sum_{k=0}^{K-1}\sqrt{p_u}N_d a_k d_{k,j_k}c_k|u_k|^2, \tag{25}$$

$$\mu_{T_{\mathrm{DP}}|\mathcal{H}_1} = \sum_{k=0}^{K-1}\sqrt{p_u}N_d a_k d_{k,j_k}b_k|u_k|^2, \tag{26}$$

$$\sigma^2_{T_{\mathrm{DP}}|\mathcal{H}_0} = \sum_{k=0}^{K-1} N_d a_k^2 d_{k,j_k} |u_k|^2 \left(p_u N_d d_{k,j_k} |u_k|^2 (1-c_k^2) + \frac{\sigma_w^2}{2} \right), \tag{27}$$

$$\sigma^2_{T_{\mathrm{DP}}|\mathcal{H}_1} = \sum_{k=0}^{K-1} N_d a_k^2 d_{k,j_k} |u_k|^2 \left(p_u N_d d_{k,j_k} |u_k|^2 (1-b_k^2) + \frac{\sigma_w^2}{2} \right). \tag{28}$$

Proof: Similar to the proof of Theorem 1. ■

In the subsequent section, the signaling vector design for the perfect CSI scenario aimed at improving the detection performance is presented.

IV. SIGNALING VECTOR DESIGN

In this section, the signaling vector $\mathbf{x} = [x_0, x_1, \ldots, x_{K-1}]^T$ is designed for maximizing the performance of the proposed C- and D-MIMO detectors. Next, the signaling vector design for the centralized architecture is presented.

A. SIGNALING VECTOR DESIGN FOR A C-MIMO BASED FC

For the signaling vector $\mathbf{u} = [u_0, u_1, \ldots, u_{K-1}]^T$, the performance can be enhanced by the deflection coefficient maximization procedure of [42], given by

$$d^2_{\mathrm{CP}}(\mathbf{u}) = \frac{(\mu_{T_{\mathrm{CP}}|\mathcal{H}_1} - \mu_{T_{\mathrm{CP}}|\mathcal{H}_0})^2}{\sigma^2_{T_{\mathrm{CP}}|\mathcal{H}_0}}. \tag{29}$$

Substituting the expressions of $\sigma^2_{T_{\mathrm{CP}}|\mathcal{H}_0}$, $\mu_{T_{\mathrm{CP}}|\mathcal{H}_1}$ and $\mu_{T_{\mathrm{CP}}|\mathcal{H}_0}$ from Theorem 1, (29) can be simplified as

$$d^2_{\mathrm{CP}}(\mathbf{u}) = \frac{\left(\sum_{k=0}^{K-1} \sqrt{p_u} M a_k d_k (b_k - c_k) |u_k|^2 \right)^2}{\sum_{k=0}^{K-1} M a_k^2 d_k |u_k|^2 \left(p_u M d_k |u_k|^2 (1 - c_k^2) + \frac{\sigma_w^2}{2} \right)}. \tag{30}$$

Consider the diagonal matrices $\Theta \in \mathbb{C}^{K\times K}$, $\Psi \in \mathbb{C}^{K\times K}$ and $\Gamma \in \mathbb{C}^{K\times K}$, where their diagonal entries are

$$[\Gamma]_{k,k} = \sqrt{p_u} M a_k d_k (b_k - c_k)^2, [\Theta]_{k,k} = \frac{1}{2} M a_k^2 d_k \sigma_w^2,$$
$$[\Psi]_{k,k} = \sqrt{p_u} M a_k d_k \sqrt{1 - c_k^2}. \tag{31}$$

Upon utilizing the above matrices, the expression in (30) can be simplified as

$$d^2_{\mathrm{CP}}(\mathbf{u}) = \frac{(\mathbf{u}^H \Gamma \mathbf{u})^2}{(\mathbf{u}^H \Psi \mathbf{u})^2 + \mathbf{u}^H \Theta \mathbf{u}}. \tag{32}$$

Observe that the above expression is non-convex, therefore, it is challenging to directly maximize (32). For finding a tractable solution, the expression in (32) can be rewritten as

$$d^2_{\mathrm{CP}}(\mathbf{u}) = \frac{\mathbf{u}^H \Lambda \mathbf{u}}{\mathbf{u}^H \Omega \mathbf{u}}, \tag{33}$$

where $\Lambda = \Gamma \mathbf{u}\mathbf{u}^H \Gamma^H$ and $\Omega = \Psi \mathbf{u}\mathbf{u}^H \Psi^H + \Theta$. Based on the Rayleigh quotient standard form, the modified objective function is

$$\max. \frac{\mathbf{u}^H \Lambda \mathbf{u}}{\mathbf{u}^H \Omega^{\frac{1}{2}} \Omega^{\frac{1}{2}} \mathbf{u}} = \max. \frac{\mathbf{v}^H \Omega^{-\frac{1}{2}} \Lambda \Omega^{-\frac{1}{2}} \mathbf{v}}{\mathbf{v}^H \mathbf{v}} = \max. \frac{\mathbf{v}^H \Xi \mathbf{v}}{\mathbf{v}^H \mathbf{v}}, \tag{34}$$

where $\Xi = \Omega^{-\frac{1}{2}} \Lambda \Omega^{-\frac{1}{2}}$ and $\mathbf{v} = \Omega^{\frac{1}{2}} \mathbf{u}$. The optimization problem in (34) can now be solved in an iterative fashion and the solution during the ith iteration is described next.

Theorem 3: To improve the detection performance of the proposed test in (14) for the centralized antenna topology, the signaling vector $\mathbf{u}^{(i)}$ of the ith iteration can be defined as $\mathbf{u}^{(i)} = (\Omega^{(i-1)})^{-\frac{1}{2}} \mathbf{v}^{(i)}$, where the ith iteration vector $\mathbf{v}^{(i)}$ can be determined from

$$\max_{\mathbf{v}^{(i)}} . \frac{\mathbf{v}^{(i)H} \Xi^{(i-1)} \mathbf{v}^{(i)}}{\mathbf{v}^{(i)H} \mathbf{v}^{(i)}}, \tag{35}$$

where $\Xi^{(i-1)} = (\Omega^{(i-1)})^{-\frac{1}{2}} \Lambda^{(i-1)} (\Omega^{(i-1)})^{-\frac{1}{2}}$ and $\mathbf{v}^{(i)} = (\Omega^{(i-1)})^{\frac{1}{2}} \mathbf{u}^{(i)}$. During the $(i-1)$st iteration, $\Omega^{(i-1)}$ and $\Lambda^{(i-1)}$ are derived by substituting $\mathbf{u}^{(i)}$ in place of $\mathbf{u}$ in (33), where $\mathbf{u}$ is initialized to $\mathbf{u}^{(0)} = \mathbf{1}_K$ during the 0th iteration.

Upon solving the optimization problem in (35), one obtains $\mathbf{v}^{(i)} = \kappa \boldsymbol{\nu}^{(i-1)}$, where the power scaling factor is κ and the eigenvector $\boldsymbol{\nu}^{(i-1)}$ of $\Xi^{(i-1)}$ is associated with the maximum eigenvalue. Therefore, the signaling vector of the ith iteration is $\mathbf{u}^{(i)} = \kappa (\Omega^{(i-1)})^{-\frac{1}{2}} \boldsymbol{\nu}^{(i-1)}$. The overall computational complexity of obtaining the signaling vector after convergence is $\mathcal{O}(nK^3)$, with K denoting the dimension of the matrix Ξ and n representing the total number of iterations. The signaling vector design for the distributed antenna topology is discussed next.

B. TRANSMIT SIGNALING VECTOR DESIGN FOR A D-MIMO BASED FC

Similarly, the ith iteration's signaling vector $\mathbf{u}_{\mathrm{D}}^{(i)}$ of the D-MIMO topology is obtained as

$$\mathbf{u}_{\mathrm{D}}^{(i)} = \alpha (\Omega_{\mathrm{D}}^{(i-1)})^{-\frac{1}{2}} \boldsymbol{\nu}_{\mathrm{D}}^{(i-1)}, \tag{36}$$

with $\boldsymbol{\nu}_{\mathrm{D}}^{(i-1)}$ as the eigenvector for the maximum eigenvalue of $\Xi_{\mathrm{D}}^{(i-1)}$ and α denoting the power scaling factor. The matrices Ω_{D} and Ξ_{D} are obtained upon replacing d_k and M by d_{k,j_k} and N_d, respectively, in (30). The asymptotic performance analysis and power scaling laws for C- and D-MIMO architectures are presented in the subsequent section.

V. ASYMPTOTIC ANALYSIS AND POWER SCALING LAWS

This section demonstrates the advantage of using a massive MIMO in distributed and centralized antenna architectures. The asymptotic performance analysis provides insights regarding the rate at which the reduction in the sensor transmit power is achieved. The asymptotic performance analysis for the centralized topology is discussed next.

A. ASYMPTOTIC PERFORMANCE OF THE C-MIMO SYSTEM

Consider the power scaling $p_u = \frac{\tilde{p}_u}{M}$, with the average sensor transmit power as $\tilde{p}_u$. For this scenario, the asymptotic detection performance of the C-MIMO test is discussed below.

Theorem 4: The asymptotic false alarm (P^a_{FA}) and detection (P^a_D) probabilities of the test in (14) for a frequency selective mmWave C-MIMO based SN are

$$P^a_D = Q\Big(\check{\gamma} - \mu^a_{T_{\mathrm{CP}}|\mathcal{H}_1}\Big), P^a_{FA} = Q\Big(\check{\gamma} - \mu^a_{T_{\mathrm{CP}}|\mathcal{H}_0}\Big),$$

where $\check{\gamma}$ is the normalized detection threshold. The normalized asymptotic means for the alternative and null hypotheses, denoted by $\mu^a_{T_{\mathrm{CP}}|\mathcal{H}_1}$ and $\mu^a_{T_{\mathrm{CP}}|\mathcal{H}_0}$, respectively, are expressed as

$$\mu^a_{T_{\mathrm{CP}}|\mathcal{H}_0} = \frac{\sum_{k=0}^{K-1}\sqrt{\tilde{p}_u}a_k d_k c_k |u_k|^2}{\sqrt{\sum_{k=0}^{K-1} a_k^2 d_k |u_k|^2\Big(\tilde{p}_u d_k |u_k|^2(1-c_k^2)+\frac{\sigma_w^2}{2}\Big)}}, \quad (37)$$

$$\mu^a_{T_{\mathrm{CP}}|\mathcal{H}_1} = \frac{\sum_{k=0}^{K-1}\sqrt{\tilde{p}_u}a_k d_k b_k |u_k|^2}{\sqrt{\sum_{k=0}^{K-1} a_k^2 d_k |u_k|^2\Big(\tilde{p}_u d_k |u_k|^2(1-b_k^2)+\frac{\sigma_w^2}{2}\Big)}}, \quad (38)$$

Proof: See Appendix B. ■

The asymptotic performance analysis for the distributed architecture is presented in the subsequent subsection.

B. ASYMPTOTIC PERFORMANCE OF THE D-MIMO SYSTEM

Considering the D-MIMO topology, the asymptotic detection (P^a_D) and false alarm (P^a_{FA}) probabilities for the test in (24), when $N_d \to \infty$ and power scaling $p_u = \frac{\tilde{p}_u}{N_d}$, are expressed as

$$P^a_D = Q\Big(\check{\gamma} - \mu^a_{T_{\mathrm{DP}}|\mathcal{H}_1}\Big), P^a_{FA} = Q\Big(\check{\gamma} - \mu^a_{T_{\mathrm{DP}}|\mathcal{H}_0}\Big),$$

where $\check{\gamma}$ is the normalized detection threshold. The normalized asymptotic means $\mu^a_{T_{\mathrm{DP}}|\mathcal{H}_1}$ and $\mu^a_{T_{\mathrm{DP}}|\mathcal{H}_0}$ for the alternative and null hypotheses, respectively, are

$$\mu^a_{T_{\mathrm{DP}}|\mathcal{H}_0} = \frac{\sum_{k=0}^{K-1}\sqrt{\tilde{p}_u}a_k d_{k,j_k} c_k |u_k|^2}{\sqrt{\sum_{k=0}^{K-1} a_k^2 d_{k,j_k} |u_k|^2\Big(\tilde{p}_u d_{k,j_k} |u_k|^2(1-c_k^2)+\frac{\sigma_w^2}{2}\Big)}},$$

$$\mu^a_{T_{\mathrm{DP}}|\mathcal{H}_1} = \frac{\sum_{k=0}^{K-1}\sqrt{\tilde{p}_u}a_k d_{k,j_k} b_k |u_k|^2}{\sqrt{\sum_{k=0}^{K-1} a_k^2 d_{k,j_k} |u_k|^2\Big(\tilde{p}_u d_{k,j_k} |u_k|^2(1-b_k^2)+\frac{\sigma_w^2}{2}\Big)}}.$$

The above expressions can be derived using similar steps to those of Theorem 4. Through the analytical expressions derived above, it is evident that one can scale the sensor transmit power as $\frac{1}{M}$ and $\frac{1}{N_d}$, for C- and D-MIMO based architectures, respectively while considering a large AA at the FC. Therefore, one can improve the sensor battery life, which is crucial for the reliable operation of next-generation SNs. The Bayesian learning (BL) based channel estimation framework for the imperfect CSI scenario is discussed in the next section.

VI. FRAMEWORK FOR SBL-BASED CSI ESTIMATION

This section discusses the frequency selective mmWave MIMO channel estimation framework using the SBL-based approach [35], [36]. Subsequently, the fusion rules are determined for both antenna topologies in the face of realistic CSI uncertainty. The sparse beamspace channel representation for the centralized architecture is discussed next.

A. SPARSE BEAMSPACE CHANNEL REPRESENTATION

To model the frequency selective mmWave MIMO channel for the C-MIMO based FC, a M size angular grid is chosen, where the AoAs are defined as $\Psi_R = \{\psi_n : \psi_n \in [0, \pi], \forall 1 \leq n \leq M\}$. Furthermore, the angles satisfy the following condition [44]

$$\sin(\psi_n) = \frac{2}{M}(n-1) - 1, \quad \forall \quad 1 \leq n \leq M. \quad (39)$$

The corresponding receive array response dictionary matrix $\mathbf{A}_{R,\mathrm{C}} \in \mathbb{C}^{M\times M}$ can be expressed as

$$\mathbf{A}_{R,\mathrm{C}} = \big[\mathbf{a}_{R,\mathrm{C}}(\psi_1), \mathbf{a}_{R,\mathrm{C}}(\psi_2), \ldots, \mathbf{a}_{R,\mathrm{C}}(\psi_M)\big]. \quad (40)$$

Owing to the selection of AoAs, the above matrix follows the property $\mathbf{A}_{R,\mathrm{C}}\mathbf{A}^H_{R,\mathrm{C}} = \mathbf{A}^H_{R,\mathrm{C}}\mathbf{A}_{R,\mathrm{C}} = \mathbf{I}_M$ [44]. Upon using the quantities defined above, the lth subcarrier's channel vector $\mathbf{g}_l \in \mathbb{C}^{M\times 1}$ can be characterized as

$$\mathbf{g}_l = \mathbf{A}_{R,\mathrm{C}}\mathbf{h}_{b,l}, \quad (41)$$

where $\mathbf{h}_{b,l} \in \mathbb{C}^{M\times 1}$ denotes its equivalent sparse beamspace channel vector. Similarly, the channel vector $\mathbf{g}_{l_j,j} \in \mathbb{C}^{N_d\times 1}, \forall l_j \in \mathbb{A}_{k_j}$, associated with the jth FC for D-MIMO is modeled as

$$\mathbf{g}_{l_j,j} = \mathbf{A}_{R,\mathrm{D}}\mathbf{h}_{b,l_j,j}, \quad (42)$$

where the equivalent sparse beamspace channel associated with the jth FC is $\mathbf{h}_{b,l_j,j} \in \mathbb{C}^{N_d\times 1}, \forall l_j \in \mathbb{A}_{k_j}$ and the receive array response dictionary matrix $\mathbf{A}_{R,\mathrm{D}} \in \mathbb{C}^{N_d\times N_d}$ is determined by using the AoAs from the set $\Psi_R = \{\psi_v : \psi_v \in [0, \pi], \forall 1 \leq v \leq N_d\}$. The BL algorithm harnessed for estimating the sparse frequency selective mmWave massive MIMO channel is presented next.

B. SBL-BASED CSI ESTIMATION

This subsection discusses the channel estimation procedure of the C-MIMO configuration, given in (41). The channel vector of the D-MIMO topology defined in (42) can be estimated using a similar approach. Let $\mathbf{x}_p \in \mathbb{C}^{K\times 1}$ be the transmitted pilot vector obeying $|x_{p,k}|^2 = 1, \forall k$, and $\mathbf{W}_{\mathrm{C}} \in \mathbb{C}^{M\times M}$ be the training RF combining matrix, which is chosen as the normalized DFT matrix of size M. For a block of N_f training frames, the channel is assumed to be constant. After

combining, the output corresponding to the lth subcarrier $\mathbf{y}^{(n)}(l) \in \mathbb{C}^{M\times 1}$ at the nth frame, becomes [41]

$$\mathbf{y}^{(n)}(l) = \sqrt{p_p}\mathbf{W}_{\mathrm{C}}^{H}\mathbf{g}_l x_{p,k}^{(n)} + \mathbf{W}_{\mathrm{C}}^{H}\mathbf{n}^{(n)}(l), \tag{43}$$

where the AWGN during the nth frame, denoted by $\mathbf{n}^{(n)}(l) \in \mathbb{C}^{M\times 1}$, follows the distribution $\mathbf{n}^{(n)}(l) \sim \mathcal{CN}(\mathbf{0}, \sigma_n^2\mathbf{I}_M)$. Upon using (41), the above expression can be simplified to

$$\mathbf{y}^{(n)}(l) = \sqrt{p_p}\Phi\mathbf{h}_{b,l}x_{p,k}^{(n)} + \tilde{\mathbf{n}}^{(n)}(l), \tag{44}$$

where $\Phi = \mathbf{W}_{\mathrm{C}}^{H}\mathbf{A}_{R,\mathrm{C}}$ and $\tilde{\mathbf{n}}^{(n)}(l) = \mathbf{W}_{\mathrm{C}}^{H}\mathbf{n}^{(n)}(l) \sim \mathcal{CN}(\mathbf{0}, \sigma_n^2\mathbf{I}_M)$. Stacking all RF combiner outputs associated with the lth subcarrier $\mathbf{y}^{(n)}(l)$, $1 \le n \le N_f$, yields

$$\mathbf{y}(l) = \sqrt{p_p}\mathbf{Q}\mathbf{h}_{b,l} + \mathbf{n}(l), \tag{45}$$

where $\mathbf{y}(l) = [(\mathbf{y}^{(1)}(l))^T, \ldots, (\mathbf{y}^{(N_f)}(l))^T]^T \in \mathbb{C}^{MN_f\times 1}$ is the stacked RF combiner output, $\mathbf{Q} = (\mathbf{x}_{p,k} \otimes \Phi) \in \mathbb{C}^{MN_f\times M}$ is the sensing matrix, and the noise $\mathbf{n}(l) = [(\tilde{\mathbf{n}}^{(1)}(l))^T, \ldots, (\tilde{\mathbf{n}}^{(N_f)}(l))^T]^T \in \mathbb{C}^{MN_f\times 1}$ is distributed as $\mathbf{n}(l) \sim \mathcal{CN}(\mathbf{0}, \mathbf{C_n})$ with $\mathbf{C_n} = \sigma_n^2\mathbf{I}_{MN_f}$. Furthermore, the columns of the sensing matrix are orthogonal, i.e., $\mathbf{Q}^H\mathbf{Q} = N_f\mathbf{I}_M$. Thus, using the received signal in (45) and the SBL framework, the lth subcarrier beamspace channel estimate $\hat{\mathbf{h}}_{b,l}$ can be obtained as follows. The proposed SBL-based framework utilizes a parameterized Gaussian prior formulated as $p(\mathbf{h}_{b,l}; \Gamma) = \mathcal{CN}(\mathbf{0}, \Gamma)$ [45], where $\Gamma = \mathrm{diag}(\gamma_1, \gamma_2, \ldots, \gamma_M)$ and the associated hyperparameter vector is defined as $\boldsymbol{\gamma} = [\gamma_1, \gamma_2, \ldots, \gamma_M]^T$. Note that here the hyperparameter $\gamma_i \in \mathbb{R}_+$ signifies the prior variance of the ith element. These hyperparameters are iteratively estimated employing the well-known expectation-maximization (EM) algorithm. The main steps in the EM procedure are summarized below.

Let $\hat{\boldsymbol{\Gamma}}^{(q)}(l)$ be the qth iteration estimate of the hyperparameter matrix $\boldsymbol{\Gamma}(l)$. In the qth iteration, the expectation step (E-step) determines the average log-likelihood $\mathcal{L}(\boldsymbol{\Gamma}(l)|\hat{\boldsymbol{\Gamma}}^{(q)}(l))$ of the data set $\{\mathbf{y}(l), \mathbf{h}_{b,l}\}$, given as

$$\mathcal{L}\big(\boldsymbol{\Gamma}(l)|\hat{\boldsymbol{\Gamma}}^{(q)}(l)\big) = \mathbb{E}_{\mathbf{h}_{b,l}|\mathbf{y}(l);\hat{\boldsymbol{\Gamma}}^{(q)}(l)}\Big\{\log\, p\big(\mathbf{y}(l), \mathbf{h}_{b,l}; \boldsymbol{\Gamma}(l)\big)\Big\}$$
$$= \mathbb{E}_{\mathbf{h}_{b,l}|\mathbf{y}(l);\hat{\boldsymbol{\Gamma}}^{(q)}(l)}\Big\{\log\, p\big(\mathbf{y}(l)|\mathbf{h}_{b,l}\big) + \log\, p\big(\mathbf{h}_{b,l}; \boldsymbol{\Gamma}(l)\big)\Big\}.$$

The first quantity in the above expression can be simplified as $-MN_f\log(\pi) - \log\,\det(\mathbf{C_n}) - (\mathbf{y}(l) - \sqrt{p_p}\mathbf{Q}\mathbf{h}_{b,l})^H\mathbf{C_n}^{-1}(\mathbf{y}(l) - \sqrt{p_p}\mathbf{Q}\mathbf{h}_{b,l})$. It can be observed that the simplified term is independent of the hyperparameter vector $\boldsymbol{\gamma}$, thus, it is ignored in the maximization step (M-step). The second term is evaluated using the *a posteriori* probability density of $\mathbf{h}_{b,l}$ [45], which is $p(\mathbf{h}_{b,l}|\mathbf{y}(l); \hat{\boldsymbol{\Gamma}}^{(q)}(l)) \sim \mathcal{CN}(\boldsymbol{\mu}^{(q)}(l), \Sigma^{(q)}(l))$ with a mean of $\boldsymbol{\mu}^{(q)}(l) = \sqrt{p_p}\Sigma^{(q)}(l)\mathbf{Q}^H\mathbf{C_n}^{-1}\mathbf{y}(l) \in \mathbb{C}^{M\times 1}$ and covariance matrix of $\Sigma^{(q)}(l) = (p_p\mathbf{Q}^H\mathbf{C_n}^{-1}\mathbf{Q} + (\widehat{\Gamma}^{(q)}(l))^{-1})^{-1} \in \mathbb{C}^{M\times M}$. Consequently, the second term reduces to

Algorithm 1: SBL-Based Frequency Selective mmWave Massive MIMO Channel Estimation

Input : Pilot output $\mathbf{y}(l)$, stopping parameter ϵ, sensing matrix $\mathbf{Q}$ and pilot power p_p.

Initialization: $\widehat{\Gamma}^{(0)}(l) = \mathbf{I}_M$

Set $q = 0$ and $\widehat{\Gamma}^{(-1)}(l) = \mathbf{0}_{M\times M}$

while $\|\hat{\boldsymbol{\Gamma}}^{(q)}(l) - \hat{\boldsymbol{\Gamma}}^{(q-1)}(l)\|_F > \epsilon$ **do**

  E-step: Determine *a posteriori* covariance and mean

    $\Sigma^{(q)}(l) = \Big(p_p\mathbf{Q}^H\mathbf{C_n}^{-1}\mathbf{Q} + \big(\widehat{\Gamma}^{(q)}(l)\big)^{-1}\Big)^{-1}$

    $\boldsymbol{\mu}^{(q)}(l) = \sqrt{p_p}\Sigma^{(q)}(l)\mathbf{Q}^H\mathbf{C_n}^{-1}\mathbf{y}(l)$

  M-step: Evaluate hyperparameter estimates

    for $i = 1, 2, \ldots, M$ **do**

      $\big[\hat{\boldsymbol{\Gamma}}^{(q+1)}(l)\big]_{i,i} = \big[\Sigma^{(q)}(l)\big]_{i,i} + \big|\big[\boldsymbol{\mu}^{(q)}(l)\big]_i\big|^2$

    end for

  $q \leftarrow q + 1$

end while

Output: $\hat{\mathbf{h}}_{b,l} = \boldsymbol{\mu}^{(q)}(l)$

$$\mathbb{E}_{\mathbf{h}_{b,l}|\mathbf{y}(l);\hat{\boldsymbol{\Gamma}}^{(q)}(l)}\Big\{\log\, p\big(\mathbf{h}_{b,l}; \boldsymbol{\Gamma}(l)\big)\Big\}$$
$$= \sum_{i=1}^{M} -\log(\pi\gamma_i) - \frac{1}{\gamma_i}\mathbb{E}_{\mathbf{h}_{b,l}|\mathbf{y}(l);\hat{\boldsymbol{\Gamma}}^{(q)}(l)}\Big\{|\mathbf{h}_{b,l}(i)|^2\Big\}. \tag{46}$$

In the M-step, the hyperparameter vector estimate $\hat{\boldsymbol{\gamma}}^{(q+1)}$is evaluated by maximizing the above cost-function with respect to $\boldsymbol{\gamma}$, as

$$\hat{\boldsymbol{\gamma}}^{(q+1)} = \underset{\boldsymbol{\gamma}}{\mathrm{argmax}}\ \mathbb{E}_{\mathbf{h}_{b,l}|\mathbf{y}(l);\hat{\boldsymbol{\Gamma}}^{(q)}(l)}\Big\{\log\, p\big(\mathbf{h}_{b,l}; \boldsymbol{\Gamma}(l)\big)\Big\}. \tag{47}$$

Observe from (46) that the estimation of the hyperparameter vector $\boldsymbol{\gamma}$ is decoupled with respect to each γ_i. Hence, it can be solved to obtain the estimates $\hat{\gamma}_i^{(q+1)}$ during the $(q+1)$st iteration of the EM algorithm as

$$\hat{\gamma}_i^{(q+1)} = \mathbb{E}_{\mathbf{h}_{b,l}|\mathbf{y}(l);\hat{\boldsymbol{\Gamma}}^{(q)}(l)}\Big\{|\mathbf{h}_{b,l}(i)|^2\Big\}$$
$$= \big[\Sigma^{(q)}(l)\big]_{i,i} + \Big|\Big[\boldsymbol{\mu}^{(q)}(l)\Big]_i\Big|^2, \tag{48}$$

where $[\Sigma^{(q)}(l)]_{i,i}$ and $[\boldsymbol{\mu}^{(q)}(l)]_i$ denote the (i,i)th and ith elements of the *a posteriori* covariance matrix $\Sigma^{(q)}(l)$ and mean vector $\boldsymbol{\mu}^{(q)}(l)$, respectively. On convergence, the SBL-based estimate is determined by substituting the hyperparameter matrix estimate $\widehat{\Gamma}$ into the *a posteriori* mean. The sparse CSI estimation technique is conveniently summarized in Algorithm 1. The fusion rule and its detection performance for the centralized topology considering imperfect CSI scenario are discussed below.

C. DECISION RULES FOR C-MIMO BASED FC WITH CSI UNCERTAINTY

Employing the technique formulated in Algorithm 1, the beamspace channel estimate of the lth subcarrier, is obtained upon convergence, as

$$\hat{\mathbf{h}}_{b,l} = \boldsymbol{\mu}^{(q)}(l), \tag{49}$$

where $\boldsymbol{\mu}^{(q)}(l)$ represents the *a posteriori* mean. Observe that the *a posteriori* covariance matrix $\Sigma_l = \Sigma^{(q)}(l)$ is diagonal, since the matrix $\widehat{\Gamma}^{(q)}(l)$ is diagonal. The mmWave massive MIMO channel estimate of the lth subcarrier is expressed as

$$\hat{\mathbf{g}}_l = \mathbf{A}_{R,\mathrm{C}}\hat{\mathbf{h}}_{b,l}, \tag{50}$$

and the beamspace estimation error is $\mathbf{e}_{b,l} = (\hat{\mathbf{h}}_{b,l} - \mathbf{h}_{b,l})$, which is distributed as $\mathbf{e}_{b,l} \sim \mathcal{CN}(\mathbf{0}, \Sigma_l)$. Hence, the corresponding estimation error $\mathbf{e}_l$ can be expressed as $\mathbf{e}_l = \hat{\mathbf{g}}_l - \mathbf{g}_l = \mathbf{A}_{R,\mathrm{C}}\mathbf{e}_{b,l}$, which is distributed as $\mathbf{e}_l \sim \mathcal{CN}(\mathbf{0}, \mathbf{C}_l)$, with $\mathbf{C}_l = \mathbf{A}_{R,\mathrm{C}}\Sigma_l\mathbf{A}_{R,\mathrm{C}}^H$. Therefore, using (5), the equivalent system model for the lth subcarrier, considering the imperfect CSI, can be remodeled as

$$\mathbf{y}(l) = \sqrt{p_u}(\hat{\mathbf{g}}_l - \mathbf{e}_l)x_k + \mathbf{w}(l) = \sqrt{p_u}\hat{\mathbf{g}}_l x_k + \bar{\mathbf{w}}(l), \tag{51}$$

where the noise $\bar{\mathbf{w}}(l) \triangleq \mathbf{w}(l) - \sqrt{p_u}\mathbf{e}_l x_k$ is distributed as $\bar{\mathbf{w}}(l) \sim \mathcal{CN}(\mathbf{0}, \sigma_w^2\mathbf{I}_M + p_u\mathbf{C}_l|u_k|^2)$ and the variables l and k are related as $k = \lfloor \frac{l}{N_s} \rfloor$. Now, a two-step procedure is conceived for reducing the computational complexity of the conventional detectors, wherein the received signal is processed using a hybrid combiner in the first step. A global decision is arrived at in the second step by fusing the hybrid combiner outputs.

The RF combiner is selected for the lth subcarrier as $\mathbf{w}_{\mathrm{RF},l} = \mathbf{a}_{R,\mathrm{C}}(\psi_{i_l})$, where i_l denotes the maximum estimated path gain index. The RF combiner output obtained by exploiting the asymptotic orthogonality property of the mmWave MIMO channel in (10) is

$$\tilde{y}(l) = \sqrt{p_u}\hat{h}_{i_l,l}x_k + \tilde{w}(l), \tag{52}$$

where $\hat{h}_{i_l,l} = [\hat{\mathbf{h}}_{b,l}]_{i_l}$ and $\tilde{w}(l) = \mathbf{w}_{\mathrm{RF},l}^H\bar{\mathbf{w}}(l)$ is distributed as $\tilde{w}(l) \sim \mathcal{CN}(0, \tilde{\sigma}_l^2)$ with $\tilde{\sigma}_l^2 = \sigma_w^2 + p_u\mathbf{w}_{\mathrm{RF},l}^H\mathbf{C}_l\mathbf{w}_{\mathrm{RF},l}|u_k|^2$. Using (52), the stacked RF combiner output $\tilde{\mathbf{y}}_k$ of the kth sensor, similar to (11), is

$$\tilde{\mathbf{y}}_k = \sqrt{p_u}\hat{\mathbf{h}}_k x_k + \tilde{\mathbf{w}}_k, \tag{53}$$

where $\tilde{\mathbf{w}}_k \sim \mathcal{CN}(\mathbf{0}, \tilde{\mathbf{C}}_k)$ and the ith diagonal entry of $\tilde{\mathbf{C}}_k$ is $[\tilde{\mathbf{C}}_k]_{i,i} = \sigma_w^2 + p_u\mathbf{w}_{\mathrm{RF},k_i}^H\mathbf{C}_{k_i}\mathbf{w}_{\mathrm{RF},k_i}|u_k|^2$ with the index $k_i = (kN_s + i - 1)$. The baseband combiner for the kth sensor is chosen as $\mathbf{w}_{\mathrm{BB},k} = \hat{\mathbf{h}}_k \in \mathbb{C}^{N_s\times 1}$ for maximizing the output SNR of the signal in (53). Thus, the digital combiner output z_k is formulated as:

$$z_k = \sqrt{p_u}\|\hat{\mathbf{h}}_k\|^2 x_k + w_k, \tag{54}$$

where the equivalent noise $w_k = \hat{\mathbf{h}}_k^H\tilde{\mathbf{w}}_k$ is distributed as $w_k \sim \mathcal{CN}(0, \sigma_k^2)$, with $\sigma_k^2 = \hat{\mathbf{h}}_k^H\tilde{\mathbf{C}}_k\hat{\mathbf{h}}_k$. Furthermore, z_k in (54) follows the distribution

$$z_k \sim \mathcal{CN}(\sqrt{p_u}\|\hat{\mathbf{h}}_k\|^2 x_k, \sigma_k^2). \tag{55}$$

Using the received signal in (54), the LLR test can be expressed as

$$T_{\mathrm{CIP}}(\mathbf{z}) = \sum_{k=0}^{K-1} \ln\left[\frac{P_{D,k} + (1-P_{D,k})\exp\left(\frac{-4\tilde{z}_k}{\sigma_k^2}\right)}{P_{F,k} + (1-P_{F,k})\exp\left(\frac{-4\tilde{z}_k}{\sigma_k^2}\right)}\right], \tag{56}$$

where we have $\tilde{z}_k = \sqrt{p_u}\|\hat{\mathbf{h}}_k\|^2\Re(z_k^* u_k)$. Upon employing the low SNR approximations of $e^{-s} \approx 1 - s$ and $\ln(1+s) \approx s$, the expression in (56) can be simplified to:

$$T_{\mathrm{CIP}}(\mathbf{z}) = \sum_{k=0}^{K-1} \frac{\|\hat{\mathbf{h}}_k\|^2}{\sigma_k^2} a_k \Re(z_k^* u_k) \underset{\mathcal{H}_0}{\overset{\mathcal{H}_1}{\gtrless}} \gamma, \tag{57}$$

where γ is the detection threshold. The above test $T_{\mathrm{CIP}}(\mathbf{z})$ represents a weighted linear combination of Gaussian random variables $\Re(z_k^* u_k)$ and it is distributed as

$$T_{\mathrm{CIP}}(\mathbf{z}) \sim \mathcal{CN}(\mu_{T_{\mathrm{CIP}}|\mathcal{H}}, \sigma^2_{T_{\mathrm{CIP}}|\mathcal{H}}), \tag{58}$$

where we have $\mathcal{H} \in \{\mathcal{H}_0, \mathcal{H}_1\}$. The expressions of the means and variances under both hypotheses can be formulated as

$$\mu_{T_{\mathrm{CIP}}|\mathcal{H}_0} = \sum_{k=0}^{K-1} \frac{\sqrt{p_u}\|\hat{\mathbf{h}}_k\|^4}{\sigma_k^2} a_k c_k |u_k|^2, \tag{59}$$

$$\mu_{T_{\mathrm{CIP}}|\mathcal{H}_1} = \sum_{k=0}^{K-1} \frac{\sqrt{p_u}\|\hat{\mathbf{h}}_k\|^4}{\sigma_k^2} a_k b_k |u_k|^2, \tag{60}$$

$$\sigma^2_{T_{\mathrm{CIP}}|\mathcal{H}_0} = \sum_{k=0}^{K-1} \frac{\|\hat{\mathbf{h}}_k\|^4}{\sigma_k^4} a_k^2 |u_k|^2 \left(p_u\|\hat{\mathbf{h}}_k\|^4|u_k|^2(1-c_k^2) + \frac{\sigma_k^2}{2}\right), \tag{61}$$

$$\sigma^2_{T_{\mathrm{CIP}}|\mathcal{H}_1} = \sum_{k=0}^{K-1} \frac{\|\hat{\mathbf{h}}_k\|^4}{\sigma_k^4} a_k^2 |u_k|^2 \left(p_u\|\hat{\mathbf{h}}_k\|^4|u_k|^2(1-b_k^2) + \frac{\sigma_k^2}{2}\right). \tag{62}$$

Based on the above quantities, the detection (P_D) and false alarm (P_{FA}) probabilities are

$$P_D = Q\left(\frac{\gamma - \mu_{T_{\mathrm{CIP}}|\mathcal{H}_1}}{\sigma_{T_{\mathrm{CIP}}|\mathcal{H}_1}}\right), P_{FA} = Q\left(\frac{\gamma - \mu_{T_{\mathrm{CIP}}|\mathcal{H}_0}}{\sigma_{T_{\mathrm{CIP}}|\mathcal{H}_0}}\right). \tag{63}$$

All the above expressions can be obtained along similar lines to those of Theorem 1. The fusion rule for the D-MIMO topology considering CSI uncertainty and its detection performance are considered next.

D. DECISION RULES FOR A D-MIMO BASED FC WITH CSI UNCERTAINTY

For the D-MIMO topology, the beamspace channel vector $\mathbf{h}_{b,l_j,j}, \forall l_j \in \mathbb{A}_{k_j}$, is estimated at each FC using the SBL-based approach. Thus, the estimated channel vector corresponding to the l_jth subcarrier at the jth FC can be expressed as

$$\hat{\mathbf{g}}_{l_j,j} = \mathbf{A}_{R,\mathrm{D}}\hat{\mathbf{h}}_{b,l_j,j}. \tag{64}$$

The estimated beamspace channel vector can be determined as $\hat{\mathbf{h}}_{b,l_j,j} = \boldsymbol{\mu}_j^{(q)}(l_j)$, where $\boldsymbol{\mu}_j^{(q)}(l_j)$ denotes the *a posteriori* mean. For the l_jth subcarrier and the jth FC, the estimation error vector can be expressed as $\mathbf{e}_{l_j,j} = \hat{\mathbf{g}}_{l_j,j} - \mathbf{g}_{l_j,j} = \mathbf{A}_{R,\mathrm{D}}\mathbf{e}_{b,l_j,j}$, which is distributed as $\mathbf{e}_{l_j,j} \sim \mathcal{CN}(\mathbf{0}, \mathbf{C}_{l_j})$, where $\mathbf{C}_{l_j} = \mathbf{A}_{R,\mathrm{D}}\Sigma_{l_j}\mathbf{A}_{R,\mathrm{D}}^H$ and Σ_{l_j} is the *a posteriori* covariance matrix. Using the above expressions, the received signal

$\mathbf{y}_j(l_j) \in \mathbb{C}^{N_d \times 1}, \forall l_j \in \mathbb{A}_{k_j}$, at the jth FC for the l_jth subcarrier, can be remodeled as

$$\begin{aligned}\mathbf{y}_j(l_j) &= \sqrt{p_u}(\hat{\mathbf{g}}_{l_j,j} - \mathbf{e}_{l_j,j})x_{k_j} + \mathbf{w}_j(l_j) \\ &= \sqrt{p_u}\hat{\mathbf{g}}_{l_j,j}x_{k_j} + \tilde{\mathbf{w}}_j(l_j),\end{aligned} \tag{65}$$

where the noise vector $\tilde{\mathbf{w}}_j(l_j) = \mathbf{w}_j(l_j) - \sqrt{p_u}\mathbf{e}_{l_j,j}x_{k_j}$ is distributed as $\tilde{\mathbf{w}}_j(l_j) \sim \mathcal{CN}(\mathbf{0}, \sigma_w^2\mathbf{I}_{N_d} + p_u\mathbf{C}_{l_j}|u_{k_j}|^2)$. Employing the two-step architecture, the RF combiner $\mathbf{w}_{\mathrm{RF},j}$ is selected as $\mathbf{w}_{\mathrm{RF},j} = \mathbf{a}_{R,\mathrm{D}}(\psi_{i_j}), \forall l_j$, which represents the receive array response vector corresponding to the maximum estimated path gain of $\hat{\mathbf{h}}_{b,l_j,j}$. The RF combiner output of the l_jth subcarrier and the jth FC obtained by leveraging the asymptotic orthogonality property of the mmWave MIMO channel, can be simplified as

$$\check{y}_j(l_j) = \sqrt{p_u}\hat{h}_{i_j,l_j,j}x_{k_j} + \check{w}_j(l_j), \tag{66}$$

where the quantities $\check{w}_j(l_j) = \mathbf{w}_{\mathrm{RF},j}^H\tilde{\mathbf{w}}_j(l_j) \sim \mathcal{CN}(0, \sigma_w^2 + p_u\mathbf{w}_{\mathrm{RF},j}^H\mathbf{C}_{l_j}\mathbf{w}_{\mathrm{RF},j}|u_{k_j}|^2)$ and $\hat{h}_{i_j,l_j,j} = [\hat{\mathbf{h}}_{b,l_j,j}]_{i_j}$. After stacking all the RF combiner outputs corresponding to the k_jth sensor, one obtains

$$\check{\mathbf{y}}_{k_j} = \sqrt{p_u}\hat{\mathbf{h}}_j x_{k_j} + \check{\mathbf{w}}_{k_j}, \tag{67}$$

where $\check{\mathbf{w}}_{k_j} \sim \mathcal{CN}(\mathbf{0}, \check{\mathbf{C}}_{k_j})$ and the covariance matrix $\check{\mathbf{C}}_{k_j}$ is diagonal with nth diagonal entry as $[\check{\mathbf{C}}_{k_j}]_{n,n} = \sigma_w^2 + p_u\mathbf{w}_{\mathrm{RF},j}^H\mathbf{C}_{n_j}\mathbf{w}_{\mathrm{RF},j}|u_{k_j}|^2$ and $n_j = k_jN_s + n - 1$. Selecting the baseband combiner vector as $\mathbf{w}_{\mathrm{BB},j} = \hat{\mathbf{h}}_j \in \mathbb{C}^{N_s \times 1}$, the hybrid combiner output of the k_jth sensor can be determined as

$$z_{k_j} = \sqrt{p_u}\|\hat{\mathbf{h}}_j\|^2 x_{k_j} + w_{k_j}, \tag{68}$$

where the quantities $w_{k_j} = \hat{\mathbf{h}}_j^H\check{\mathbf{w}}_{k_j} \sim \mathcal{CN}(0, \sigma_{k_j}^2)$ and $\sigma_{k_j}^2 = \hat{\mathbf{h}}_j^H\check{\mathbf{C}}_{k_j}\hat{\mathbf{h}}_j$. The hybrid combiner outputs are then transmitted to the BPU for final processing. At the BPU, the correction matrix $\mathbf{S}$ is used to combine the received signals to obtain ordered soft sensor decisions. Thus, the hybrid combined output signal of the kth sensor can be given as

$$z_k = \sqrt{p_u}\|\hat{\mathbf{h}}_{j_k}\|^2 x_k + w_k, \tag{69}$$

where the quantities $w_k \sim \mathcal{CN}(0, \sigma_k^2)$ and $\sigma_k^2 = \hat{\mathbf{h}}_{j_k}^H\check{\mathbf{C}}_k\hat{\mathbf{h}}_{j_k}$. Further, z_k in (69) is distributed as

$$z_k \sim \mathcal{CN}(\sqrt{p_u}\|\hat{\mathbf{h}}_{j_k}\|^2 x_k, \sigma_k^2). \tag{70}$$

Using (69), the LLR test statistic for $\mathbf{z}$, considering the D-MIMO topology, can be modeled as

$$T_{\mathrm{DIP}}(\mathbf{z}) = \sum_{k=0}^{K-1}\frac{\|\hat{\mathbf{h}}_{j_k}\|^2}{\sigma_k^2}a_k\Re(z_k^*u_k) \underset{\mathcal{H}_0}{\overset{\mathcal{H}_1}{\gtrless}} \check{\gamma}, \tag{71}$$

where $\check{\gamma}$ is the detection threshold. Furthermore, the expressions of P_D and P_{FA} for $T_{\mathrm{DIP}}(\mathbf{z})$ in (71) can be derived as

$$P_D = Q\left(\frac{\gamma - \mu_{T_{\mathrm{DIP}}|\mathcal{H}_1}}{\sigma_{T_{\mathrm{DIP}}|\mathcal{H}_1}}\right), P_{FA} = Q\left(\frac{\gamma - \mu_{T_{\mathrm{DIP}}|\mathcal{H}_0}}{\sigma_{T_{\mathrm{DIP}}|\mathcal{H}_0}}\right),$$

where the means $\mu_{T_{\mathrm{DIP}}|\mathcal{H}_0}$, $\mu_{T_{\mathrm{DIP}}|\mathcal{H}_1}$ and the variances $\sigma^2_{T_{\mathrm{DIP}}|\mathcal{H}_0}$, $\sigma^2_{T_{\mathrm{DIP}}|\mathcal{H}_1}$ under null and alternative hypotheses, respectively, are determined as

$$\begin{aligned}
\mu_{T_{\mathrm{DIP}}|\mathcal{H}_0} &= \sum_{k=0}^{K-1}\frac{\sqrt{p_u}\|\hat{\mathbf{h}}_{j_k}\|^4}{\sigma_k^2}a_kc_k|u_k|^2, \\
\mu_{T_{\mathrm{DIP}}|\mathcal{H}_1} &= \sum_{k=0}^{K-1}\frac{\sqrt{p_u}\|\hat{\mathbf{h}}_{j_k}\|^4}{\sigma_k^2}a_kb_k|u_k|^2, \\
\sigma^2_{T_{\mathrm{DIP}}|\mathcal{H}_0} &= \sum_{k=0}^{K-1}\frac{\|\hat{\mathbf{h}}_{j_k}\|^4}{\sigma_k^4}a_k^2|u_k|^2\left(p_u\|\hat{\mathbf{h}}_{j_k}\|^4|u_k|^2(1-c_k^2)+\frac{\sigma_k^2}{2}\right), \\
\sigma^2_{T_{\mathrm{DIP}}|\mathcal{H}_0} &= \sum_{k=0}^{K-1}\frac{\|\hat{\mathbf{h}}_{j_k}\|^4}{\sigma_k^4}a_k^2|u_k|^2\left(p_u\|\hat{\mathbf{h}}_{j_k}\|^4|u_k|^2(1-c_k^2)+\frac{\sigma_k^2}{2}\right), \\
\sigma^2_{T_{\mathrm{DIP}}|\mathcal{H}_1} &= \sum_{k=0}^{K-1}\frac{\|\hat{\mathbf{h}}_{j_k}\|^4}{\sigma_k^4}a_k^2|u_k|^2\left(p_u\|\hat{\mathbf{h}}_{j_k}\|^4|u_k|^2(1-b_k^2)+\frac{\sigma_k^2}{2}\right).
\end{aligned}$$

The proof of the above expressions follows along similar lines to Theorem 1. The simulation results to validate the proposed analyses are discussed in the subsequent section.

VII. SIMULATION RESULTS

This section demonstrates the simulation results to corroborate the analytical performance of the C- and D-MIMO detectors and to contrast their performance to those of other detectors. For the C-MIMO configuration, $K = 16$ sensors are uniformly distributed in the range spanning from r_{min} to R, where $r_{min} = 1$ m and $R = 200$ m. In the D-MIMO architecture, $J = 16$ FCs are located on a circle of radius $\rho = 0.6R$ and $K = 16$ sensors are uniformly distributed in the region $[0, \rho - r_{min}] \cup [\rho + r_{min}, R]$. The system under consideration is operating at $f_c = 28$ GHz and the antenna spacing is chosen as $d = \lambda/2$. The local false alarm and detection probabilities are taken as $P_{F,k} \sim \mathcal{U}[0.01, 0.16]$ and $P_{D,k} \sim \mathcal{U}[0.2, 0.95]$, respectively. The frequency selective mmWave massive MIMO channel is considered to be spatially sparse with $L_k = L_{k,j} = 4$ paths and $D = 4$ delay taps. The classic raised cosine pulse shaping filter is utilized with a roll-off factor of 0.6 and the delays $\tau_{k,i}$ are chosen uniformly in the range $[0, D-1]$. The large-scale fading coefficients of the C- and D-MIMO topologies are modeled similar to [40], as $\beta_k = \frac{\nu_k}{(\rho_k/r_{min})^\nu}$ and $\beta_{k,j} = \frac{\nu_{k,j}}{(d_{k,j}/r_{min})^\nu}$, respectively. The quantities ν_k and $\nu_{k,j}$ are generated as log-normal random variables with a mean of $\mu_\nu = 4$ dB and standard deviation of $\sigma_\nu = 2$ dB. Furthermore, ρ_k and $d_{k,j}$ denote the distance from the kth sensor to the centralized FC and the jth FC for the C-and D-MIMO configurations, respectively, and $\nu = 2$. The noise variances are set to $\sigma_w^2 = \sigma_n^2 = 1$.

Fig. 5(a) demonstrates the effect of varying the number of subcarriers assigned to each sensor, i.e., $N_s \in \{1, 2, 4\}$, on the receiver operating characteristic (ROC) plot of the C-MIMO detector in (14) for $M = 256$ and $p_u = -10$ dB.

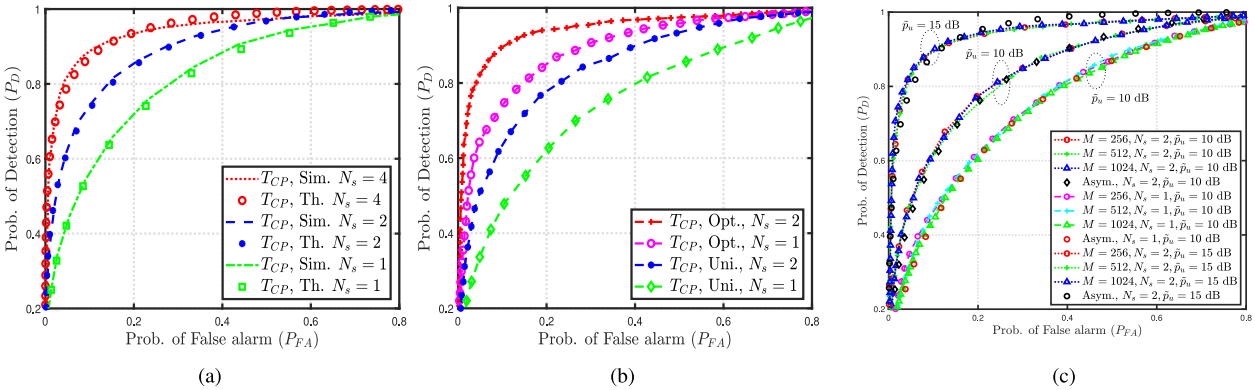

FIGURE 5. ROC plots of the C-MIMO based test $T_{CP}(\mathbf{z})$ in (14), a) Theoretical and simulated ROC with $M = 256$, $N_s \in \{1, 2, 4\}$ and $p_u = -10$ dB, b) Performance with and without signaling vector design with $M = 256$, $N_s \in \{1, 2\}$ and $p_u = -15$ dB, c) Asymptotic performance analysis for with $M \in \{256, 512, 1024\}$, $N_s \in \{1,2\}$ and $\tilde{p}_u \in \{10,15\}$ dB.

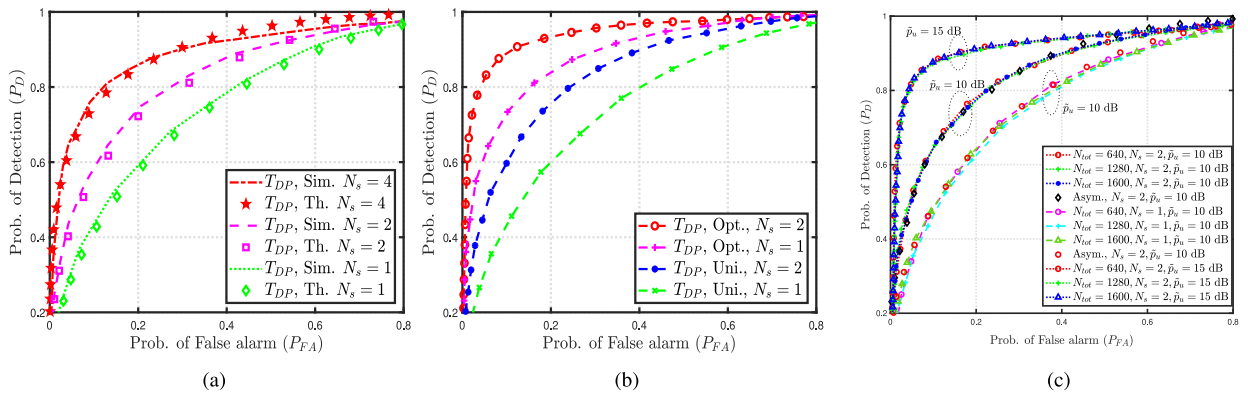

FIGURE 6. ROC plots of the D-MIMO based test $T_{DP}(\mathbf{z})$ in (24), a) Theoretical and simulated ROC with $N_{tot} = 1024$, $N_s \in \{1, 2, 4\}$ and $p_u = -5$ dB, b) Performance with and without signaling vector design with $N_{tot} = 1024$, $N_s \in \{1, 2\}$ and $p_u = -5$ dB, c) Asymptotic performance analysis for with $N_{tot} \in \{640, 1280, 1600\}$, $N_s \in \{1,2\}$ and $\tilde{p}_u = 10$ dB.

Observe that the simulated plots coincide with the analytical findings derived, thus validating the accuracy of our analysis. Moreover, the performance improves upon increasing the values of N_s. Thus, one can fine-tune the number of subcarriers according to the detection performance desired. Fig. 5(b) compares the detection performance obtained using the signaling vector designed in Section IV to that of a uniform transmit signaling vector design, wherein all the sensors transmit at equal power, i.e., $\mathbf{u} = [u_0, u_1, \ldots, u_{K-1}]^T$, where $u_k \in \{-1, 1\}$, for $p_u = -15$ dB. Observe from the figure that one can significantly enhance the detection performance by employing the transmit signaling vector, which demonstrates the value of our optimal signaling paradigm conceived for practical mmWave massive MIMO-OFDM systems. Fig. 5(c) verifies the power scaling laws determined in Section V for a centralized mmWave massive MIMO-OFDM system. As shown therein, the figure supports our conclusion that the sensor transmit power can be reduced according to $1/M$, without affecting the detection performance. This key result pertaining to the asymptotic performance analysis helps us in improving the battery life of the sensors, which is one of the critical resources in a WSN. Moreover, the detection performance improves with an increase in the value of $\tilde{p}_u$.

The ROC plot of the proposed D-MIMO test in (24) is depicted in Fig. 6(a) for $N_s \in \{1, 2, 4\}$, considering $N_{tot} = 1024$ and $p_u = -5$ dB. The analytical results derived in Theorem 2 are also verified using the simulation results. The performance improves as N_s increases and the capability of the scheme can be further enhanced by employing the deflection coefficient maximization-based signaling vector, as demonstrated in Fig. 6(b). When contrasting Fig. 5(a) and Fig. 6(a), the performance degradation in D-MIMO against C-MIMO is attributed to the sensor distribution range. The asymptotic performance of the test in (24) with power scaling is explored in Fig. 6(c). Observe that one can scale the sensor transmit power as $1/N_d$, for the D-MIMO topology.

Fig. 7(a) portrays the performance of the C- and D-MIMO based tests of (14) and (24), respectively, considering $N_s \in \{1, 2\}$, $M = N_{tot} = 1024$, $P_{FA} = 0.1$, $p_u = -10$ dB and sensor position range $[0.5R, R]$. Notice that the performance is enhanced as the density of sensors increases. Moreover, the D-MIMO detector outperforms the C-MIMO detector owing to an increase in the number of FCs deployed upon increasing the sensor density. Considering $M = N_{tot} = 1024$, $P_{FA} = 0.1$ and $p_u = -10$ dB, it becomes clear from Fig. 7(b) that the D-MIMO detector's performance is maximized at $\rho/R = 0.6$. This happens because for $\rho/R = 0.6$, the sensors

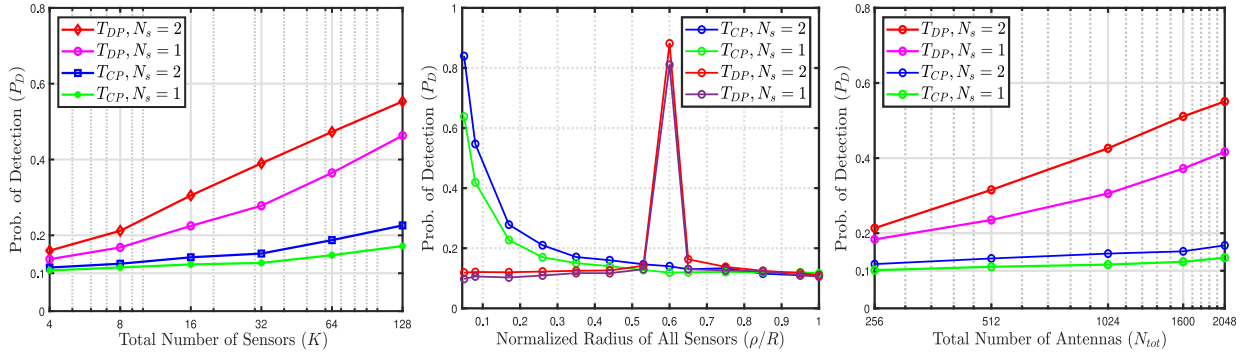

FIGURE 7. Performance comparison of the C-MIMO and D-MIMO based detectors, derived in (14) and (24), respectively, with $N_s \in \{1, 2\}$ a) P_D vs. K, with $N_{tot} = 1024$ and $p_u = -10$ dB, b) P_D vs. normalized radius of all sensors (ρ/R), with $N_{tot} = 1024$ and $p_u = -5$ dB c) P_D vs. N_{tot} at the FC, with $p_u = -5$ dB.

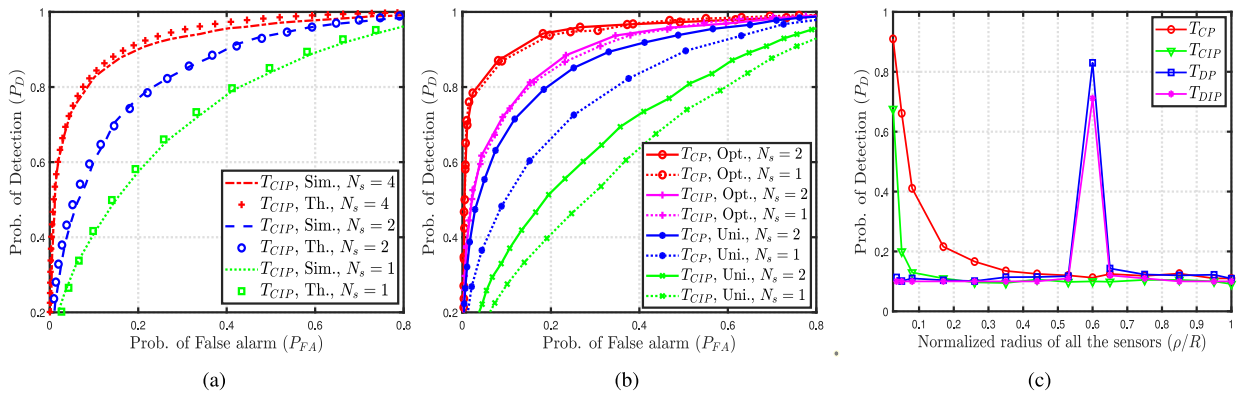

FIGURE 8. a) Theoretical and simulation ROC plots of the C-MIMO detector for the imperfect CSI scenario in (57), with $M = 256$, $N_s \in \{1, 2, 4\}$, $p_u = -15$ dB, $p_p = 8$ dB and $N_f = 12$, b) Performance comparison of uniform and deflection coefficient maximization based signaling vector for C-MIMO detectors for the perfect and imperfect CSI scenarios, derived in (14) and (57), respectively, with $M = 256$, $N_s \in \{1, 2\}$, $p_u = -10$ dB and $p_p = -5$ dB, c) P_D vs. normalized radius of the sensors (ρ/R) for C-MIMO and D-MIMO detectors, proposed in (14) and (24), (57) and (71), corresponding to the perfect and imperfect CSI scenarios, with $N_{tot} = 1024$, $N_s = 1$, $p_u = -10$ dB, $p_p = -5$ dB and $N_f = 12$ at $P_{FA} = 0.1$.

are nearest to their associated FCs. Furthermore, observe from Fig. 7(c) that the detection probability P_D improves as the total number of antennas grows, for $P_{FA} = 0.1$ and $p_u = -10$ dB. Clearly, the D-MIMO outperforms the C-MIMO in terms of its detection performance for sensor positions in the range $[0.5R, R]$.

Upon considering the centralized topology, the performance of the SBL-based detector of (57) is analyzed in Fig. 8(a) for the scenario of imperfect CSI, for $N_s \in \{1, 2, 4\}$, $M = 256$, $p_u = -15$ dB, pilot power $p_p = 8$ dB and number of frames $N_f = 12$. The simulation results validate accuracy of the theoretical results derived in (63). The performance of the C-MIMO based detectors, derived in (14) and (57), is contrasted in Fig. 7b, for the perfect and imperfect CSI scenarios, respectively, for $N_s \in \{1, 2\}$, $p_u = -10$ dB and $p_p = -5$ dB. It is evident from the figure that the performance of both detectors improves by increasing the number of subcarriers of each sensor, which can be further improved by employing the proposed signaling vectors. But naturally, there is a clear diversity vs. throughput trade-off. Fig. 8(c) analyzes the performance of the C- and D-MIMO detectors, proposed in (14), (24), (57) and (71), for the perfect and imperfect CSI scenarios, respectively. The parameters are chosen as $N_s = 1$, $N_{tot} = 1024$, $p_u = -10$ dB, $p_p = -5$ dB, $P_{FA} = 0.1$ and $N_f = 12$, for the sensor allocation range $[0.5R, R]$. Observe that the D-MIMO detector outperforms its C-MIMO equivalent. Thus, one can overcome the shortcomings of the C-MIMO based topology by exploiting the benefits of the distributed antenna configuration.

The performance of the D-MIMO based detectors, derived in (24) and (71) for the perfect and imperfect CSI scenarios is shown in Fig. 9(a) and Fig. 9(b). It can be observed that the P_D performance of distributed detection can be improved by assigning an increased number of subcarriers to the sensors coupled with transmit signaling vector design. However, at a given total bandwidth, limiting the number of subcarriers limits the total system throughput. Fig. 9(c) shows the variation of P_D versus the pathloss exponent (ν), for the D-MIMO based architecture, considering $N_s = 1$, $N_{tot} \in \{512, 1024, 2048\}$, $p_u = -10$ dB, $p_p = 0$ dB, $P_{FA} = 0.1$ and $N_f = 12$. An increase in ν degrades the P_D performance, which can be alleviated by using a large antenna array at the FC.

VIII. CONCLUSION

Hybrid combining based detection rules were developed for distributed detection in frequency selective mmWave

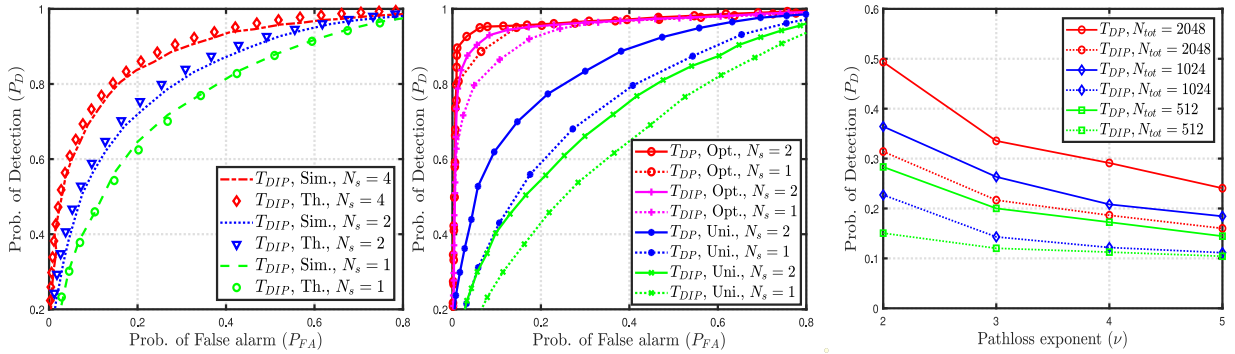

FIGURE 9. a) Theoretical and simulated ROC plots for D-MIMO detector in (71), for imperfect CSI, considering N_{tot}= *1024*, p_u= *−10* dB and p_p= *10* dB, b) Performance comparison of uniform and deflection coefficient maximization based signaling vector for D-MIMO based detectors in (24) and (71), for perfect and imperfect CSI, respectively, with N_{tot}= *1024*, p_u= *−7* dB and p_p= *0* dB, c) P_D vs. pathloss exponent (ν) comparison of the D-MIMO system for the perfect and imperfect CSI scenarios, with $N_{tot} \in$ *{512, 1024, 2048}*, N_s= *1*, p_u= *−10* dB, p_p= *0* dB, P_{FA}= *0.1* and N_f= *12*.

massive MIMO SNs, employing D- and C-MIMO antenna topologies, where the local sensor decisions are transmitted to the FC over orthogonal subcarriers. For this framework, the decision rules were designed for the perfect CSI scenario and their performance was characterized via explicit analytical expressions for the resultant false alarm and detection probabilities. Furthermore, signaling vectors were obtained based on the deflection coefficient maximization criterion for both antenna topologies to improve the detection performance. The asymptotic performance and the power reduction laws were also characterized for demonstrating the rate at which the sensors can reduce their transmit power when the number of antennas at the FC becomes very large. Additionally, an SBL-based sparse mmWave massive MIMO CSI estimation procedure was developed followed by the associated fusion rules conceived for distributed detection under CSI uncertainty, for both antenna configurations. A comprehensive set of simulation results was presented to validate the performance of the proposed algorithms. Future research will prioritize the exploration of distributed detection in scenarios that take into account the allocation of multiple sensors per FC within the distributed antenna topology. Additionally, there is potential for further investigations into multi-cell scenarios.

APPENDIX A
PROOF OF THEOREM 1

Substituting the expression of z_k from (12) in (14), one obtains

$$T_{\mathrm{CP}}(\mathbf{z}) = \sum_{k=0}^{K-1} a_k \Re(\sqrt{p_u} M d_k x_k^* u_k + w_k^* u_k). \tag{72}$$

The mean of $T_{\mathrm{CP}}(\mathbf{z})$ for hypothesis $\mathcal{H}_0$ is

$$\begin{aligned}\mu_{T_{\mathrm{CP}}|\mathcal{H}_0} &= \mathbb{E}\{T_{\mathrm{CP}}(\mathbf{z})|\mathcal{H}_0\} \\ &= \sum_{k=0}^{K-1} a_k \Re\Big(\sqrt{p_u} M d_k \mathbb{E}\{x_k^*|\mathcal{H}_0\} u_k + \mathbb{E}\{w_k^*|\mathcal{H}_0\} u_k\Big).\end{aligned}$$

Further, the quantities $\mathbb{E}\{x_k^*|\mathcal{H}_0\} = P_{F,k} u_k^* - (1 - P_{F,k}) u_k^* = c_k u_k^*$, where $c_k = 2P_{F,k} - 1$ and $\mathbb{E}\{w_k^*|\mathcal{H}_0\} = 0$. On substituting the above expressions, $\mu_{T_{\mathrm{CP}}|\mathcal{H}_0}$ can be simplified as

$$\mu_{T_{\mathrm{CP}}|\mathcal{H}_0} = \sum_{k=0}^{K-1} \sqrt{p_u} M a_k d_k c_k |u_k|^2. \tag{73}$$

The variance in (17) can be derived as $\sigma^2_{T_{\mathrm{CP}}|\mathcal{H}_0} = \mathbb{E}\{T^2_{\mathrm{CP}}(\mathbf{z})|\mathcal{H}_0\} - \mu^2_{T_{\mathrm{CP}}|\mathcal{H}_0}$, where $\mathbb{E}\{T^2_{\mathrm{CP}}(\mathbf{z})|\mathcal{H}_0\}$ is

$$\begin{aligned}\mathbb{E}\{T^2_{\mathrm{CP}}(\mathbf{z})|\mathcal{H}_0\} &= \mathbb{E}\left\{\left(\sum_{k=0}^{K-1} a_k \Re(\sqrt{p_u} M d_k x_k^* u_k + w_k^* u_k)\right)^2 \middle| \mathcal{H}_0\right\} \\ &= \sum_{k=0}^{K-1} a_k^2 |u_k|^2 \left(p_u M^2 d_k^2 \mathbb{E}\{|x_k|^2|\mathcal{H}_0\} + \frac{\sigma_k^2}{2}\right) \\ &= \sum_{k=0}^{K-1} a_k^2 |u_k|^2 \left(p_u M^2 d_k^2 |u_k|^2 + \frac{M d_k \sigma_w^2}{2}\right),\end{aligned}$$

where $\mathbb{E}\{|w_k|^2|\mathcal{H}_0\} = \sigma_k^2 = M d_k \sigma_w^2$. Therefore, the variance $\sigma^2_{T_{\mathrm{CP}}|\mathcal{H}_0}$ can be expressed as

$$\sigma^2_{T_{\mathrm{CP}}|\mathcal{H}_0} = \sum_{k=0}^{K-1} M a_k^2 d_k |u_k|^2 \left(p_u M d_k |u_k|^2 (1 - c_k^2) + \frac{\sigma_w^2}{2}\right). \tag{74}$$

Similarly, the mean and variance can be obtained for $T_{\mathrm{CP}}(\mathbf{z})$ in (72) under hypothesis $\mathcal{H}_1$.

APPENDIX B
PROOF OF THEOREM 4

Consider the modified test statistic $\tilde{T}_{\mathrm{CP}}(\mathbf{z}) = \frac{T_{\mathrm{CP}}(\mathbf{z})}{\sigma_{T_{\mathrm{CP}}|\mathcal{H}_0}} \sim \mathcal{CN}(\tilde{\mu}_{T_{\mathrm{CP}}|\mathcal{H}_0}, 1)$, where $\tilde{\mu}_{T_{\mathrm{CP}}|\mathcal{H}_0} = \frac{\mu_{T_{\mathrm{CP}}|\mathcal{H}_0}}{\sigma_{T_{\mathrm{CP}}|\mathcal{H}_0}}$ denotes the normalized mean under the null hypothesis. For the power scaling $p_u = \frac{\tilde{p}_u}{M}$, with the average sensor transmit power as $\tilde{p}_u$, the normalized asymptotic mean for hypothesis $\mathcal{H}_0$ can be determined as

$$\mu^a_{T_{\mathrm{CP}}|\mathcal{H}_0} = \lim_{M\to\infty} \tilde{\mu}_{T_{\mathrm{CP}}|\mathcal{H}_0}\Big|_{p_u = \frac{\tilde{p}_u}{M}}. \tag{75}$$

On substituting the expressions of $\mu_{T_{\mathrm{CP}}|\mathcal{H}_0}$ and $\sigma_{T_{\mathrm{CP}}|\mathcal{H}_0}$ from (15) and (17) in (75), the above expression reduces to

$$\mu^a_{T_{\mathrm{CP}}|\mathcal{H}_0} = \frac{\sum_{k=0}^{K-1} \sqrt{\tilde{p}_u} a_k d_k c_k |u_k|^2}{\sqrt{\sum_{k=0}^{K-1} a_k^2 d_k |u_k|^2 \left(\tilde{p}_u d_k |u_k|^2 (1-c_k^2) + \frac{\sigma_w^2}{2}\right)}}. \quad (76)$$

On similar lines, one can obtain the normalized asymptotic mean under hypothesis $\mathcal{H}_1$.

REFERENCES

[1] I. Akyildiz, W. Su, Y. Sankarasubramaniam, and E. Cayirci, "Wireless sensor networks: A survey," *Comput. Netw.*, vol. 38, no. 4, pp. 393–422, 2002.

[2] Z. Sheng, C. Mahapatra, C. Zhu, and V. C. M. Leung, "Recent advances in industrial wireless sensor networks toward efficient management in IoT," *IEEE Access*, vol. 3, pp. 622–637, 2015.

[3] R. V. Kulkarni and G. K. Venayagamoorthy, "Particle swarm optimization in wireless-sensor networks: A brief survey," *IEEE Trans. Syst., Man, Cybern. C, Appl. Rev.*, vol. 41, no. 2, pp. 262–267, Mar. 2011.

[4] R. Viswanathan and P. K. Varshney, "Distributed detection with multiple sensors part I. Fundamentals," *Proc. IEEE*, vol. 85, no. 1, pp. 54–63, Jan. 1997.

[5] I. A. Hemadeh, K. Satyanarayana, M. El-Hajjar, and L. Hanzo, "Millimeter-wave communications: Physical channel models, design considerations, antenna constructions, and link-budget," *IEEE Commun. Surveys Tuts.*, vol. 20, no. 2, pp. 870–913, 2nd Quart., 2018.

[6] T. S. Rappaport, E. Ben-Dor, J. N. Murdock, and Y. Qiao, "38 GHz and 60 GHz angle-dependent propagation for cellular peer-to-peer wireless communications," in *Proc. IEEE Int. Conf. Commun. (ICC)*, Jun. 2012, pp. 4568–4573.

[7] S. Sun, T. S. Rappaport, R. W. Heath, A. Nix, and S. Rangan, "MIMO for millimeter-wave wireless communications: Beamforming, spatial multiplexing, or both?" *IEEE Commun. Mag.*, vol. 52, no. 12, pp. 110–121, Dec. 2014.

[8] S. Han, I. Chih-Lin, Z. Xu, and C. Rowell, "Large-scale antenna systems with hybrid analog and digital beamforming for millimeter wave 5G," *IEEE Wireless Commun. Mag.*, vol. 53, no. 1, pp. 186–194, Jan. 2015.

[9] J. Li, D.-W. Yue, and Y. Sun, "Performance analysis of millimeter wave massive MIMO systems in centralized and distributed schemes," *IEEE Access*, vol. 6, pp. 75482–75494, 2018.

[10] W. Li and H. Dai, "Distributed detection in wireless sensor networks using a multiple access channel," *IEEE Trans. Signal Process.*, vol. 55, no. 3, pp. 822–833, Mar. 2007.

[11] F. Li and J. S. Evans, "Design of distributed detection schemes for multiaccess channels," in *Proc. Aust. Commun. Theory Workshop*, Jan. 2008, pp. 51–57.

[12] C. Tepedelenlioglu and S. Dasarathan, "Distributed detection over Gaussian multiple access channels with constant modulus signaling," *IEEE Trans. Signal Process.*, vol. 59, no. 6, pp. 2875–2886, Jun. 2011.

[13] C. R. Berger, M. Guerriero, S. Zhou, and P. Willett, "PAC vs. MAC for decentralized detection using noncoherent modulation," *IEEE Trans. Signal Process.*, vol. 57, no. 9, pp. 3562–3575, Sep. 2009.

[14] D. Ciuonzo, G. Romano, and P. Salvo Rossi, "Optimality of received energy in decision fusion over Rayleigh fading diversity MAC with non-identical sensors," *IEEE Trans. Signal Process.*, vol. 61, no. 1, pp. 22–27, Jan. 2013.

[15] M. K. Banavar, A. D. Smith, C. Tepedelenlioğlu, and A. Spanias, "Distributed detection over fading MACs with multiple antennas at the fusion center," in *Proc.IEEE ICASSP*, Mar. 2010, pp. 2894–2897.

[16] M. K. Banavar, A. D. Smith, C. Tepedelenlioglu, and A. Spanias, "On the effectiveness of multiple antennas in distributed detection over fading MACs," *IEEE Trans. Wireless Commun.*, vol. 11, no. 5, pp. 1744–1752, May 2012.

[17] D. Ciuonzo, G. Romano, and P. S. Rossi, "Channel-aware decision fusion in distributed MIMO wireless sensor networks: Decode-and-fuse vs. decode-then-fuse," *IEEE Trans. Wireless Commun.*, vol. 11, no. 8, pp. 2976–2985, Aug. 2012.

[18] I. Nevat, G. W. Peters, and I. B. Collings, "Distributed detection in sensor networks over fading channels with multiple antennas at the fusion centre," *IEEE Trans. Signal Process.*, vol. 62, no. 3, pp. 671–683, Feb. 2014.

[19] M. A. Al-Jarrah, A. Al-Dweik, M. Kalil, and S. S. Ikki, "Decision fusion in distributed cooperative wireless sensor networks," *IEEE Trans. Veh. Technol.*, vol. 68, no. 1, pp. 797–811, Jan. 2019.

[20] A. Patel, H. Ram, A. K. Jagannatham, and P. K. Varshney, "Robust cooperative spectrum sensing for MIMO cognitive radio networks under CSI uncertainty," *IEEE Trans. Signal Process.*, vol. 66, no. 1, pp. 18–33, Jan. 2018.

[21] F. Jiang, J. Chen, A. L. Swindlehurst, and J. A. López-Salcedo, "Massive MIMO for wireless sensing with a coherent multiple access channel," *IEEE Trans. Signal Process.*, vol. 63, no. 12, pp. 3005–3017, Jun. 2015.

[22] S. A. Astaneh and S. Gazor, "Frequency domain distributed OFDM source detection," in *Proc. 5th IEEE Int. Workshop Comput. Adv. Multi-Sens. Adapt. Process. (CAMSAP)*, Dec. 2013, pp. 380–383.

[23] A. Chawla, A. Patel, A. K. Jagannatham, and P. K. Varshney, "Distributed detection in massive MIMO wireless sensor networks under perfect and imperfect CSI," *IEEE Trans. Signal Process.*, vol. 67, no. 15, pp. 4055–4068, Aug. 2019.

[24] A. Chawla, A. S. Sarode, A. K. Jagannatham, and L. Hanzo, "Distributed parameter detection in massive MIMO wireless sensor networks relying on imperfect CSI," *IEEE Trans. Wireless Commun.*, vol. 20, no. 1, pp. 506–519, Jan. 2021.

[25] A. Chawla, R. K. Singh, A. Patel, and A. K. Jagannatham, "Distributed detection in millimeter wave massive MIMO wireless sensor networks," in *Proc. Int. Conf. Signal Process. Commun. (SPCOM)*, Jul. 2020, pp. 1–5.

[26] A. Chawla, R. K. Singh, A. Patel, A. K. Jagannatham, and L. Hanzo, "Distributed detection for centralized and decentralized millimeter wave massive MIMO sensor networks," *IEEE Trans. Veh. Technol.*, vol. 70, no. 8, pp. 7665–7680, Aug. 2021.

[27] A. Chawla, P. S. Kumar, S. Srivastava, and A. K. Jagannatham, "Centralized and distributed millimeter wave massive MIMO-based data fusion with perfect and Bayesian learning (BL)-based imperfect CSI," *IEEE Trans. Commun.*, vol. 70, no. 3, pp. 1777–1791, Mar. 2022.

[28] A. Chawla, D. Ciuonzo, and P. S. Rossi, "Sparse Bayesian learning assisted decision fusion in millimeter wave massive MIMO sensor networks," in *Proc. IEEE Int. Conf. Acoust., Speech Signal Process. (ICASSP)*, 2023, pp. 1–5.

[29] S. Gimenez, D. Calabuig, S. Roger, J. Monserrat, and N. Cardona, "Distributed hybrid precoding for indoor deployments using millimeter wave band," *Mobile Inf. Syst.*, vol. 2017, Oct. 2017, Art. no. 5751809

[30] D. Castanheira, P. Lopes, A. Silva, and A. Gameiro, "Hybrid beamforming designs for massive MIMO millimeter-wave heterogeneous systems," *IEEE Access*, vol. 5, pp. 21806–21817, 2017.

[31] W. Tang and L. Wang, "Cooperative OFDM for energy-efficient wireless sensor networks," in *Proc. IEEE Workshop Signal Process. Syst.*, Oct. 2008, pp. 77–82.

[32] M. A. Al-Jarrah, N. K. Al-Ababneh, M. M. Al-Ibrahim, and R. A. Al-Jarrah, "Cooperative OFDM for semi distributed detection in wireless sensor networks," *AEU Int. J. Electron. Commun.*, vol. 68, no. 10, pp. 1022–1029, 2014.

[33] R. Xu, "Density function of the received signal in OFDM-based distributed detection fusion system," *Int. J. Wireless Inf. Netw.*, vol. 22, pp. 357–368, Sep. 2015.

[34] F. Jiang, J. Chen, and A. L. Swindlehurst, "Estimation in phase-shift and forward wireless sensor networks," *IEEE Trans. Signal Process.*, vol. 61, no. 15, pp. 3840–3851, Aug. 2013.

[35] D. P. Wipf and B. D. Rao, "Sparse Bayesian learning for basis selection," *IEEE Trans. Signal Process.*, vol. 52, no. 8, pp. 2153–2164, Aug. 2004.

[36] S. Srivastava, A. Mishra, A. Rajoriya, A. K. Jagannatham, and G. Ascheid, "Quasi-static and time-selective channel estimation for block-sparse millimeter wave hybrid MIMO systems: Sparse Bayesian learning (SBL) based approaches," *IEEE Trans. Signal Process.*, vol. 67, no. 5, pp. 1251–1266, Mar. 2019.

[37] S. Srivastava, R. K. Singh, A. K. Jagannatham, and L. Hanzo, "Bayesian learning aided sparse channel estimation for orthogonal time frequency space modulated systems," *IEEE Trans. Veh. Technol.*, vol. 70, no. 8, pp. 8343–8348, Aug. 2021.
[38] D. Yue and H. H. Nguyen, "Multiplexing gain analysis of mmWave massive MIMO systems with distributed antenna subarrays," *IEEE Trans. Veh. Technol.*, vol. 68, no. 11, pp. 11368–11373, Nov. 2019.
[39] S. Park, A. Alkhateeb, and R. W. Heath, "Dynamic subarrays for hybrid precoding in wideband mmWave MIMO systems," *IEEE Trans. Wireless Commun.*, vol. 16, no. 5, pp. 2907–2920, May 2017.
[40] H. Q. Ngo, E. G. Larsson, and T. L. Marzetta, "Energy and spectral efficiency of very large multiuser MIMO systems," *IEEE Trans. Commun.*, vol. 61, no. 4, pp. 1436–1449, Apr. 2013.
[41] J. P. González-Coma, J. Rodríguez-Fernández, N. González-Prelcic, L. Castedo, and R. W. Heath, "Channel estimation and hybrid precoding for frequency selective multiuser mmwave MIMO systems," *IEEE J. Sel. Topics Signal Process.*, vol. 12, no. 2, pp. 353–367, May 2018.
[42] S. M. Kay, *Fundamentals of Statistical Signal Processing: Detection Theory*, vol. 2. Hoboken, NJ, USA: Prentice-Hall, Inc., 1993.
[43] S. Zhou, W. Xu, H. Zhang, and X. You, "Hybrid precoding for millimeter wave massive MIMO with analog combining," in *Proc. 9th Int. Conf. Wireless Commun. Signal Process. (WCSP)*, Oct. 2017, pp. 1–5.
[44] J. Lee, G. Gil, and Y. H. Lee, "Channel estimation via orthogonal matching pursuit for hybrid MIMO systems in millimeter wave communications," *IEEE Trans. Commun.*, vol. 64, no. 6, pp. 2370–2386, Jun. 2016.
[45] M. E. Tipping, "Sparse Bayesian learning and the relevance vector machine," *J. Mach. Learn. Res.*, vol. 1, pp. 211–244, Sep. 2001.

PALLA SIVA KUMAR (Student Member, IEEE) received the M.Tech. degree in electrical engineering from the Indian Institute of Technology Kanpur, Kanpur, India, in 2021. He is currently working as a Senior Engineer with Qualcomm India Pvt. Ltd., Hyderabad, where the area of work focuses mainly on the digital transceiver radio frequency platform interface. In addition to that, he worked on the baseband processing of 2G GSM/GPRS/EGPRS/EDGE technologies. His research interests include compressive sensing, distributed detection, signal processing, and wireless communication.

APOORVA CHAWLA (Member, IEEE) received the B.Tech. degree in electronics and communication engineering from Gautam Buddh Technical University, India, in 2012, and the M.Tech.–Ph.D. dual degree in electrical engineering from the Indian Institute of Technology Kanpur, Kanpur, India, in 2022. She is currently a Postdoctoral Researcher with the Department of Electronic Systems, Norwegian University of Science and Technology, Trondheim, Norway. Her research interests include distributed detection, massive MIMO, mmWave communication, sensor validation, machine learning, and signal processing. She was awarded the TCS Research Fellowship for pursuing graduate studies at the Indian Institute of Technology Kanpur. In 2019, she was selected as one of the finalists for the Qualcomm Innovation Fellowship by Qualcomm, India.

SURAJ SRIVASTAVA (Member, IEEE) received the M.Tech. degree in electronics and communication engineering from the Indian Institute of Technology Roorkee, India, in 2012, and the Ph.D. degree in electrical engineering from the Indian Institute of Technology Kanpur, India, in 2022. He is currently an Assistant Professor with the Department of Electrical Engineering, Indian Institute of Technology Jodhpur. From July 2012 to November 2013, he was employed as a Staff-I Systems Design Engineer with Broadcom Research India Pvt. Ltd., Bengaluru, and from November 2013 to December 2015, he was employed as a Lead Engineer with Samsung Research India, Bengaluru, where he worked on developing layer-2 of the 3G UMTS/WCDMA/HSDPA modem. He worked as a senior lead engineer in Qulacomm India Pvt. Ltd., Bengaluru, from October 2022 to November 2023. His research interests include applications of sparse signal processing in 5G wireless systems, mmWave and terahertz communication, orthogonal time–frequency space, joint radar and communication, optimization, and machine learning. He was awarded the Qualcomm Innovation Fellowship in 2018 and 2022 from Qualcomm. He was also awarded the Outstanding Ph.D. Thesis and Outstanding Teaching Assistant awards from IIT Kanpur.

ADITYA K. JAGANNATHAM (Senior Member, IEEE) received the bachelor's degree from the Indian Institute of Technology Bombay, Mumbai, India, and the M.S. and Ph.D. degrees from the University of California at San Diego, San Diego, CA, USA. From 2007 to 2009, he was employed as a Senior Wireless Systems Engineer with Qualcomm Inc., San Diego, where he was a part of the Qualcomm CDMA Technologies Division. He is currently a Professor with the Department of Electrical Engineering, Indian Institute of Technology Kanpur, Kanpur, India, where he also holds the Arun Kumar Chair Professorship. His research interests include next-generation wireless cellular and WiFi networks, with a special emphasis on various 5G technologies, such as massive MIMO, mmWave MIMO, FBMC, NOMA, and emerging 6G technologies, such as OTFS, IRS, THz systems, and VLC. He has been twice awarded the P. K. Kelkar Young Faculty Research Fellowship for excellence in research, and received multiple Qualcomm Innovation Fellowships in 2018 and 2022. He was the recipient of the IIT Kanpur Excellence in Teaching Award, the CAL(IT)2 Fellowship at the University of California at San Diego, the Upendra Patel Achievement Award at Qualcomm San Diego, and the Qualcomm 6G UR India Gift.

LAJOS HANZO (Life Fellow, IEEE) received the first Honorary Doctorate degree from the Technical University of Budapest in 2009, and the second Honorary Doctorate degree from Edinburgh University in 2015. He holds the IEEE Eric Sumner Technical Field Award. He is a Foreign Member of the Hungarian Science-Academy, a Fellow of the Royal Academy of Engineering, IET, and EURASIP. For further details, please see http://www-mobile.ecs.soton.ac.uk and https://en.wikipedia.org/wiki/Lajos_Hanzo.